Development 139, 667-677 (2012) doi:10.1242/dev.072272

Genetic ablation of *Rest* leads to in vitro-specific derepression of neuronal genes during neurogenesis

Hitomi Aoki[1], Akira Hara[2], Takumi Era[3], Takahiro Kunisada[1] and Yasuhiro Yamada[4,5,*]

SUMMARY

Rest (RE1-silencing transcription factor, also called Nrsf) is involved in the maintenance of the undifferentiated state of neuronal stem/progenitor cells in vitro by preventing precocious expression of neuronal genes. However, the function of *Rest* during neurogenesis in vivo remains to be elucidated because of the early embryonic lethal phenotype of conventional *Rest* knockout mice. In the present study, we have generated *Rest* conditional knockout mice, which allow the effect of genetic ablation of *Rest* during embryonic neurogenesis to be examined in vivo. We show that *Rest* plays a role in suppressing the expression of neuronal genes in cultured neuronal cells in vitro, as well as in non-neuronal cells outside of the central nervous system, but that it is dispensable for embryonic neurogenesis in vivo. Our findings highlight the significance of extrinsic signals for the proper intrinsic regulation of neuronal gene expression levels in the specification of cell fate during embryonic neurogenesis in vivo.

KEY WORDS: Rest (Nrsf), Mouse model, Neurogenesis

INTRODUCTION

The establishment and maintenance of neuronal identity underlie the core of neuronal development. The transcriptional repressor RE1-silencing transcription factor [Rest; also known as neuron-restrictive silencer factor (Nrsf)], was initially discovered as a negative regulator of neuron-specific genes in non-neuronal cells (Chong et al., 1995; Schoenherr and Anderson, 1995). Rest is expressed throughout early development, where it represses the expression of neuronal genes and is involved in the transcriptional silencing of neuronal promoters in conjunction with CoRest (Rcor1/2) (Ballas et al., 2001), which recruits additional silencing machinery, including the methyl DNA-binding protein MeCP2, histone deacetylase (HDAC) and the histone H3K9 methyltransferase G9a (Ehmt2) (Andres et al., 1999; Lunyak et al., 2002; Roopra et al., 2004; Shi et al., 2003; You et al., 2001). Rest targets include a number of genes encoding ion channels, neurotrophins, synaptic vesicle proteins and neurotransmitter receptors (Bruce et al., 2004; Johnson et al., 2006; Otto et al., 2007). Indeed, a targeted mutation of *Rest* in mice caused derepression of neuron-specific tubulin in a subset of non-neuronal tissues, leading to embryonic lethality (Chen et al., 1998).

Mosaic inhibition of *Rest* in chicken embryos using a dominant-negative form of *Rest* also caused derepression of neuronal tubulin, as well as several other neuronal target genes, not only in non-neuronal tissues but also neuronal progenitors (Chen et al., 1998). These results suggest that *Rest* is required to repress the expression of neuronal genes in undifferentiated neuronal tissue. Expression of Rest is highest in embryonic stem cells (ESCs) and is downregulated as ESCs differentiate into neuronal stem cells (NSCs), and it is completely silenced in mature adult neuronal cells (Ballas et al., 2005). Given the fact that Rest represses the expression of a large number of neuronal genes, it is reasonable to expect that it plays a central role in the inhibition of the precocious expression of neuronal genes in NSCs, and that its downregulation upon receipt of neuronal differentiation cues permits the robust expression of differentiation-related neuronal genes, resulting in terminal differentiation (Ballas et al., 2005).

In addition to the involvement of Rest in neurogenesis, recent studies have demonstrated that Rest modulates glial lineage elaboration (Abrajano et al., 2009; Kohyama et al., 2010), suggesting that it also mediates the coupling of neurogenesis and gliogenesis, which might contribute to the neuronal-glial interactions that are associated with synaptic and neuronal network plasticity and homeostasis in the brain. Despite the expectation of a fundamental role of Rest in brain development, the function of Rest in NSCs and neuronal progenitors in the brain in vivo remains to be elucidated. *Rest* null mice survive to embryonic day (E) 9 without obvious morphological defects, by which time all three germ layers and the neural tube have formed, clearly demonstrating that neuronal progenitors can develop in vivo in the absence of *Rest* (Chen et al., 1998). However, *Rest* null mice die by E11.5 accompanied by gross morphological changes starting ~E9.5. This early embryonic lethality has precluded further analysis of the role of *Rest* in the maintenance and differentiation of NSCs and neural progenitor cells (NPCs) in vivo.

In addition to the possible role of *Rest* in neuronal/glial development, recent studies have indicated that the breakdown of these processes accompanies and promotes neurodegenerative disorders. The disruption of the interaction of Rest with its target genes was reported in epileptic seizures (Bassuk et al., 2008), Huntington's disease (Zuccato et al., 2007) and Down's syndrome (Canzonetta et al., 2008; Lepagnol-Bestel et al., 2009). In these disorders, Rest dysfunction is suggested to be a cause of aberrant changes in neuronal gene expression. Considering that abnormal expression of Rest has been seen in a variety of neurological and neurodegenerative diseases, it is important to uncover the

[1]Department of Tissue and Organ Development and [2]Department of Tumor Pathology, Regeneration, and Advanced Medical Science, Gifu University Graduate School of Medicine, Gifu, 501-1194, Japan. [3]Division of Molecular Neurobiology, Institute of Molecular Embryology and Genetics, Kumamoto University, Kumamoto 860-0811, Japan. [4]PRESTO, Japan Science and Technology Agency, 4-1-8 Honcho Kawaguchi, Saitama, Japan. [5]Center for iPS Cell Research and Application (CiRA), Institute for Integrated Cell-Material Sciences (iCeMS), Kyoto University, Kyoto 606-8507, Japan.

*Author for correspondence (y-yamada@cira.kyoto-u.ac.jp)

Accepted 18 December 2011

mechanisms that underlie how Rest suppresses the expression of neuronal genes to control neurogenesis and gliogenesis, and to provide a better understanding of the pathogenesis of such diseases.

In the present study, we have generated *Rest* conditional knockout mice that allow the effects of genetic ablation of *Rest* on brain development to be examined in vivo. We also examined the effect of *Rest* ablation in cells outside of the nervous system at different developmental stages.

MATERIALS AND METHODS

Animals

All animal experiments were approved by the Animal Research Committee of the Gifu University Graduate School of Medicine. *Rest*$^{2lox/2lox}$ mice were generated from the *Rest*$^{2lox/+}$ ESC line as described preciously (Yamada et al., 2010). *Rosa26::rtTA*; *Col1a1::tetO-Cre* mice (Yamada et al., 2010) and *Sox1-Cre/+* mice (Takashima et al., 2007) were bred with *Rest*$^{2lox/2lox}$ mice to generate compound transgenic mice. In order to induce Cre recombinase, doxycycline (2 mg/ml) was administered in the drinking water of the mice, supplemented with 10 mg/ml sucrose (Hochedlinger et al., 2005). To induce Cre-*loxP* recombination in the embryos, pregnant female mice were treated with doxycycline in their drinking water for 5 days, and were sacrificed on the last day of the doxycycline administration. In order to label neuronal stem/progenitor cells in the adult brain, BrdU was administered as a daily intraperitoneal injection of 50 mg/kg body weight for 12 days starting at the age of 8 weeks. The brains were fixed 1 day after the last injection (Shi et al., 2004).

Cell culture

For the neurosphere culture, brains were collected and dissociated into single-cell suspensions by gentle pipetting. The inner part of the trunk region was collected for genotyping. The primary neurospheres were formed from 1×10^5 suspended brain cells/well in a 24-well plate. The cells were cultured in DMEM/F12 supplemented with 1× N2 (Invitrogen), 1× B27 (Invitrogen), 20 ng/ml epidermal growth factor (EGF) (R&D Systems) and 20 ng/ml basic fibroblast growth factor (bFGF, or FGF2) (R&D Systems). The primary neurospheres were passaged to generate secondary neurospheres, which were used to compare neurosphere formation ability. For the adherent cultures of neurospheres, the spheres were inoculated into 6-well plates previously coated with fibronectin/laminin (both from Invitrogen) and cultured in DMEM/F12 supplemented with 1× B27 and 10% fetal calf serum (FCS) (Nichirei Bioscience, Tokyo, Japan).

MEFs were derived from small pieces of the outer part of the trunk region prepared as described above. The cells were seeded in 100-mm dishes and cultured in DMEM supplemented with 10% FCS. In order to induce *Rest* recombination in vitro, cultured cells were treated with doxycycline at 2 μg/ml. The cells were analyzed for GFP signals using a FACS Aria dual-laser flow cytometer (Becton-Dickinson).

Histology and immunohistochemistry

The brains were enucleated and fixed by immersion overnight in 10% formalin in phosphate buffer (pH 7.2). Specimens were dehydrated with ethanol, soaked in xylene and embedded in paraffin. Horizontal serial sections were prepared at 3μm using a Leica RM2125RT microtome and stained with Hematoxylin and Eosin (HE).

For immunohistochemistry, we used a Mouse-to-Mouse HRP Ready-To-Use Kit (ScyTek Laboratories) according to the manufacturer's protocol to detect the mouse monoclonal primary antibodies on the sections. For detection of the goat or rabbit polyclonal primary antibodies, a Histofine Kit (Nichirei Bioscience, Tokyo, Japan) or VECTASTAIN ABC Kit (Vector Laboratories) was used according to the manufacturers' protocol. Finally, the sections were stained with 3,3′-diaminobenzidine (DAB). For immunocytochemistry studies, cells were fixed with 4% PFA, made permeable by immersion in 0.1% Triton X-100, washed in PBS and blocked in 0.5% BSA. Primary antibodies were then added and allowed to react for 60 minutes at room temperature. After washing in PBS, the cells were stained with secondary antibodies. Cells were examined using an Olympus IX-71 fluorescence microscope.

Antibodies

The primary antibodies used in this study were: anti-mouse neuronal class III beta-tubulin (Tuj1; 1:5000; BabCO); anti-mouse glial fibrillary acidic protein (Gfap; 1:1000; Dako-Cytomation, Glostrup, Denmark); anti-human nestin (1:500; IBL, Gunma, Japan); anti-mouse nestin (1:1000; Chemicon); anti-mouse NeuN (1:1000; Chemicon); anti-BrdU (1:500; Dako-Cytomation); anti-doublecortin (Dcx; 1:500; Santa Cruz); anti-Prox1 (1:5000; Millipore); anti-radial glial cell marker 2 (clone RC2; 1:300; Millipore); anti-trimethyl histone H3 (Lys27) (1:200; Monoclonal Institute, Hokkaido, Japan).

Gene expression analysis

Total RNA was prepared using the RNeasy Plus Mini Kit (Qiagen) according to the manufacturer's instructions. The first-strand cDNA was synthesized from 1 μg total RNA using the SuperScript First-Strand Synthesis System (Takara, Shiga, Japan) with oligo(dT) primers. Real-time PCR was performed with SYBR Premix EX Taq (Takara) using Thermal Cycler Dice (Takara) for each gene of interest, and a β-actin endogenous control primer set was used for normalization. The primer sequences used in qRT-PCR analyses were obtained from PrimerBank (http://pga.mgh.harvard.edu/primerbank/).

The microarray analysis was performed according to the manufacturer's instructions (materials from Agilent unless otherwise stated). Briefly, cyanine-3 (Cy3)-labeled cRNA was prepared from 100 ng RNA using the One-Color Low RNA Input Liner Amplification Kit, followed by RNeasy column purification (Qiagen). Dye incorporation and cRNA yield were checked with a NanoDrop ND-1000 spectrophotometer. A total of 1.5 μg of Cy3-labeled cRNA (specific activity >10.0 pmol Cy3/μg cRNA) was fragmented at 60°C for 30 minutes in a reaction volume of 50 μl containing 1× fragmentation buffer and 2× blocking agent following the manufacturer's instructions. On completion of the fragmentation reaction, 50 μl 2× HI-RPM Hybridization Buffer was added and hybridized to Whole Mouse Genome Oligo Microarrays (G4122F) for 17 hours at 65°C in a rotating hybridization oven. After hybridization, microarrays were washed for 1 minute at room temperature with GE Wash Buffer 1 and 1 minute at 37°C with GE Wash buffer 2, then dried immediately by brief centrifugation. Slides were scanned immediately after washing on a DNA microarray scanner (G2565B) using the one-color scan setting for 4×44k array slides [scan area 75×25 mm, scan resolution 5 μm, dye channel set to green and green PMT set to 10-100% (XDR)]. The scanned images were analyzed with the Feature Extraction Software package v. 9.5.3.1 using default parameters (protocol GE1-v5_95_Feb07 and Grid: 014868_D_F_20101102) to obtain background-subtracted and spatially detrended processed signal intensities. Data were analyzed using GeneSpring software.

RESULTS

Conditional ablation of the CoRest binding site in developing embryos results in embryonic lethality

In order to examine the effect of *Rest* deletion in vivo, we generated mice containing floxed *Rest* alleles and doxycycline-inducible *Cre* alleles (*Rest*$^{2lox/2lox}$; *Rosa26::rtTA*; *Col1a1::tetO-Cre*), in which exon 4, which encodes the CoRest binding site, can be removed upon treatment of mice with doxycycline (Fig. 1A) (Andres et al., 1999; Beard et al., 2006; Fink et al., 1999; Hatano et al., 2011; Yamada et al., 2010). Rest contains two repressor domains (Tapia-Ramirez et al., 1997): an N-terminal domain that associates with HDACs and Sin3; and a C-terminal domain that interacts with CoRest (Andres et al., 1999). Importantly, although our recombined *Rest* knockout (KO) allele (*Rest*^{1lox}) still contains exons 1-3, which encode the N-terminal domain of Rest, altered *Rest* transcript was not detected in our *Rest*$^{1lox/1lox}$ mouse ESCs, suggesting that the *Rest*^{1lox} allele in this system is equivalent to the conventional KO allele (Yamada et al., 2010). We further demonstrated that *Stmn2* (*SCG10*), a CoRest-independent target of Rest-mediated repression (Jepsen et al., 2000; Lunyak et al., 2002),

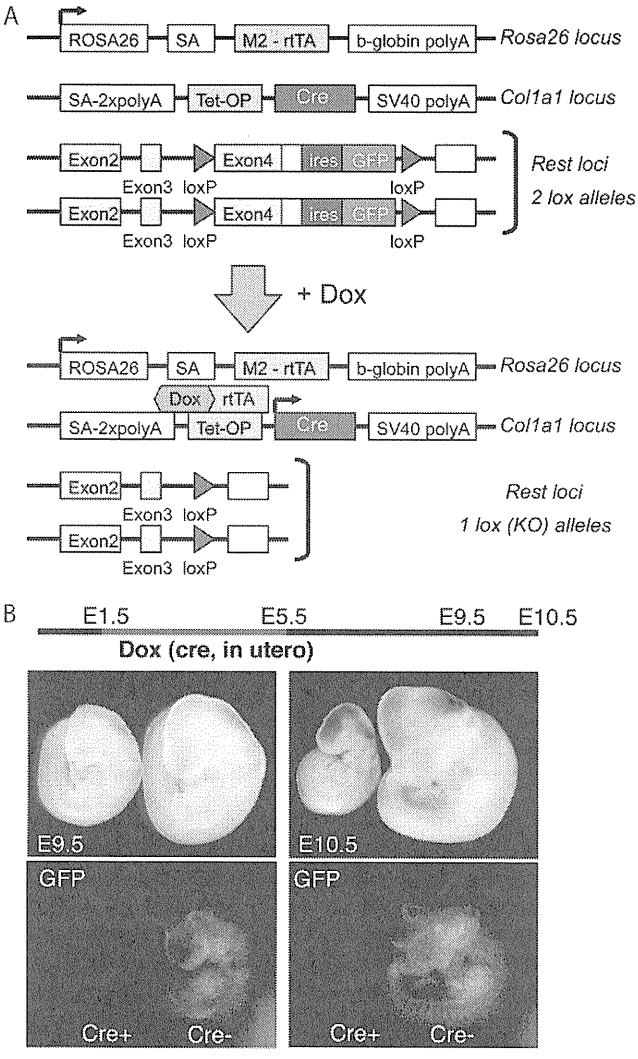

Fig. 1. Conditional *Rest* knockout mice. (**A**) In the conditional *Rest* knockout (KO) mice, exon 4 of *Rest* can be removed by doxycycline (Dox) exposure. (**B**) Pregnant mice with *Rest* conditional KO embryos were treated with doxycycline to delete the *Rest* alleles from the embryos in utero (E1.5-5.5). The growth retardation phenotype is detectable at E9.5 and E10.5.

is upregulated in $Rest^{1lox/1lox}$ mouse ESCs (supplementary material Fig. S1), indicating again that our *Rest* KO cells are equivalent to the *Rest* null cells.

A previous study using conventional KO mice revealed that mice lacking the *Rest* gene die during early embryonic development (Chen et al., 1998). When we administrated doxycycline to the *Rest* conditional KO embryos to delete the *Rest* gene in utero (E1.5-5.5), we observed lethality of the embryos carrying the *tetO-Cre* allele at ~E10.5 with a growth retardation phenotype, which was accompanied by the loss of GFP signals, indicating that the phenotype of the conventional KO mice could be recapitulated in our *Rest* conditional KO mice (Fig. 1B).

Genetic ablation of *Rest* in non-neuronal cells outside of the central nervous system in vitro

Previous studies suggest that *Rest* is expressed in a variety of non-neuronal cells to suppress the neuronal differentiation of these cells. Indeed, the conventional *Rest* KO mice showed ectopic expression of Rest target genes, such as *Tuj1* (*Tubb3*), in non-neuronal cells outside of the brain (Chen et al., 1998). Therefore, to elucidate whether *Rest* ablation can induce the expression of Rest target genes in non-neuronal cells, we used mouse embryonic fibroblasts (MEFs) containing floxed *Rest* alleles and doxycycline-inducible *Cre* alleles ($Rest^{2lox/2lox}$; *Rosa26*::*rtTA*; *Col1a1*::*tetO-Cre*). The *Rest* conditional KO MEFs were treated with doxycycline for 3 days starting 1 day after the seeding of the MEFs (passage 1). Seven days after the seeding of the MEFs, the MEFs were examined for GFP expression by FACS analysis. Three weeks after the seeding of the MEFs, they were analyzed by immunocytochemistry with a Tuj1 antibody to detect expression of the neural cell marker. The expression of Rest target genes was also examined by real-time RT-PCR 3 weeks after the seeding of the MEFs.

Consistent with the recombination, FACS analysis revealed a decreased GFP signal in the *Rest* conditional KO MEFs treated with doxycycline (Fig. 2A). As demonstrated in a previous study using conventional KO mice, deletion of *Rest* caused an increase in the expression of Tuj1 in MEFs (Fig. 2B) (Chen et al., 1998). The real-time RT-PCR revealed that MEFs treated with doxycycline expressed a significantly reduced level of *GFP* and *Rest* (Fig. 2C). We found that this was associated with increased expression of *Syt4*, *Tubb3* and *Calb1*, which contain RE1 sites and are targets of the Rest repressor complex (Chong et al., 1995; Johnson et al., 2008; Schoenherr and Anderson, 1995; Schoenherr et al., 1996) (Fig. 2C). We also found that *Stmn2*, a CoRest-independent target of Rest-mediated repression, was also derepressed in MEFs by doxycycline exposure (Fig. 2C). These results indicate that Rest target genes are rapidly derepressed upon the loss of *Rest* in MEFs. However, *Bdnf*, which also contains an RE1 site and is a target of the Rest repressor complex in ESCs/NSCs (Johnson et al., 2008; Yamada et al., 2010), did not show any detectable derepression in doxycycline-treated MEFs (Fig. 2C).

Although we confirmed that removal of the *Rest* CoRest binding site induces ectopic neuronal gene expression in non-neuronal cells outside of the brain, it remains unclear whether *Rest* ablation can actually induce neuronal differentiation in non-neuronal cells. In the present study, despite the observed increase in the expression of neuronal genes such as *Syt4*, *Tubb3*, *Calb1* and *Stmn2* after ablation of *Rest* in MEFs, the morphology of the Tuj1-expressing cells did not change (Fig. 2B). In addition, the expression of *Fsp1* (*S100a4*), a marker for fibroblasts (Strutz et al., 1995), was not decreased in the Tuj1-expressing MEFs (supplementary material Fig. S2). These findings suggest that *Rest* ablation in non-neuronal cells leads to ectopic neuronal gene expression, but that its ablation is not sufficient to induce transdifferentiation into neuronal cells (Vierbuchen et al., 2010).

We also examined the effect of *Rest* ablation in adult non-neuronal cells in vitro using tail tip fibroblasts (TTFs) containing the floxed *Rest* alleles and doxycycline-inducible *Cre* alleles. After exposure to doxycycline, we detected significant upregulation of the Rest target genes *Syt4*, *Tubb3*, *Calb1* and *Stmn2* in the TTFs, which was accompanied by the downregulation of *Rest* and *GFP* expression (supplementary material Fig. S3). Consistent with the results in MEFs, we failed to detect derepression of *Bdnf* or downregulation of *Fsp1* in TTFs after *Rest* ablation (supplementary material Fig. S3). We also conditionally deleted the *Rest* CoRest binding site in adult mice by the administration of doxycycline in the drinking water, and examined the expression of Rest target genes in the tail tissues. We confirmed the derepression of Rest target genes in the adult tail tissues after genetic ablation of *Rest* in vivo (supplementary material Fig. S4).

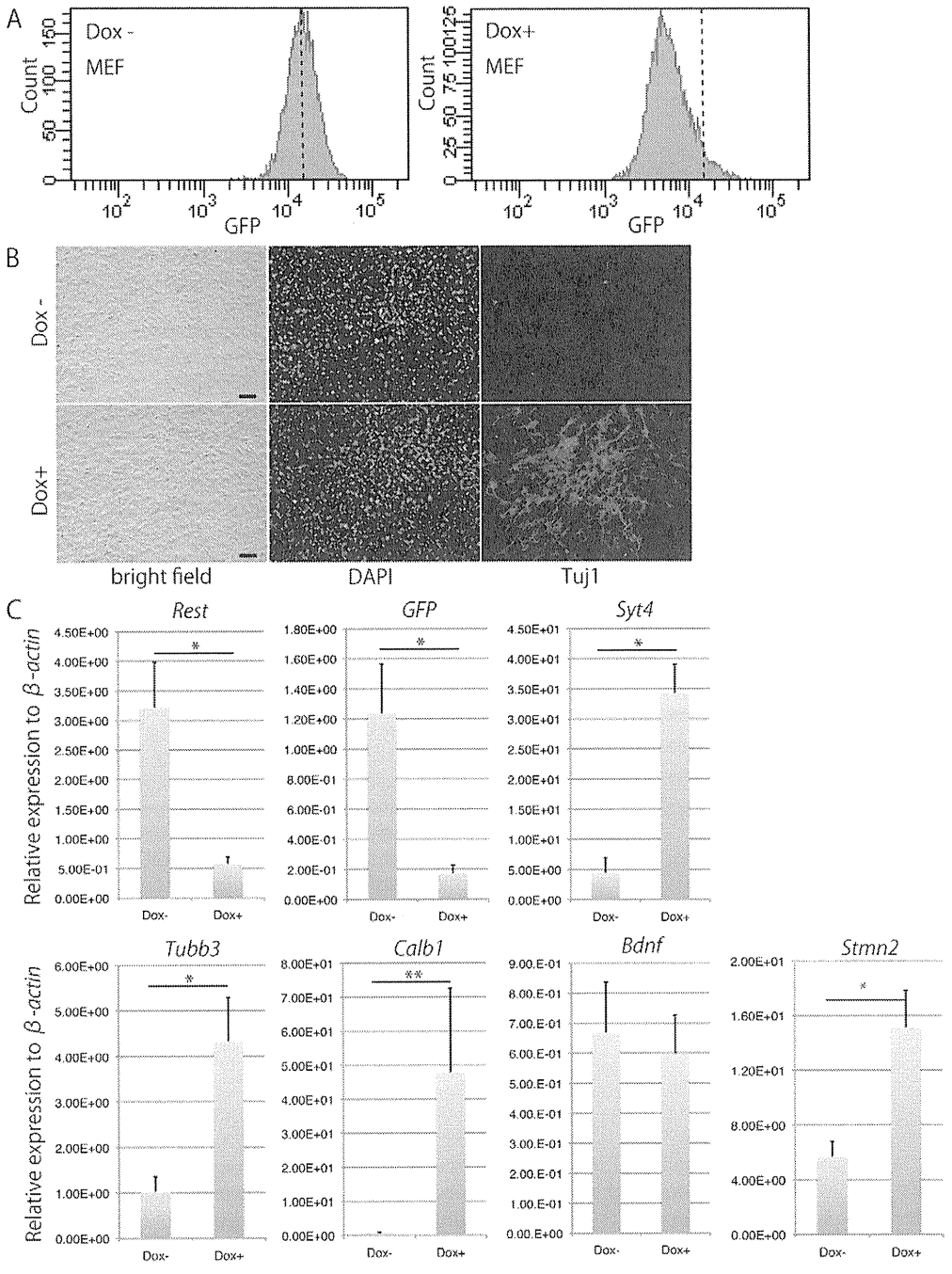

Fig. 2. The conditional deletion of *Rest* in mouse embryonic fibroblasts leads to derepression of Rest target genes. (**A**) FACS analysis revealed a decreased signal for GFP fluorescence in doxycycline-treated mouse embryonic fibroblasts (MEFs) 7 days after seeding of the MEFs. The dashed line indicates the GFP signal at the peak of the histogram of the control cells for comparison. (**B**) The conditional deletion of *Rest* in MEFs resulted in an increased number of Tuj1-positive cells in vitro. Tuj1 expression was also observed in some postmitotic neuronal cells with long axons, which were likely to be contaminating neuronal cells present in the MEF culture. Scale bars: 100 μm. (**C**) Transcript levels of *Rest*, *GFP* and Rest target genes. The expression levels of the Rest target genes *Syt4*, *Tubb3*, *Calb1* and *Stmn2* were significantly upregulated, whereas the expression levels of *Rest* and *GFP* were downregulated after *Rest* ablation in MEFs. No significant change was detectable in the *Bdnf* expression level. Transcript levels were normalized to β-actin levels. The data are presented as average values with s.d. of nine independent samples. *, $P<0.00001$; **, $P<0.0005$.

In vitro ablation of *Rest* in neuronal progenitor cells

Rest is downregulated in the brain as gestation progresses (Ballas et al., 2005). We first examined the expression of *Rest* in the developing mouse brain. The conditional KO alleles contain IRES-*GFP* sequences at the 3′ UTR of the *Rest* gene, which enable us to detect the expression and distribution of *Rest* by the GFP signals. By analyzing GFP expression, we confirmed that cells in the brain at E13.5 actually express the *Rest* gene (Fig. 3A).

In order to investigate the effect of genetic ablation of *Rest* during neurogenesis in vitro, we generated neurospheres from the brains of E13.5 *Rest* conditional KO embryos carrying the doxycycline-inducible *Cre* alleles. The primary neurospheres were passaged to form secondary neurospheres. Doxycycline was administered for 3 days starting 1 day after the passage of the primary neurospheres (passage 1). When we measured the number of secondary neurospheres in order to compare the formation of neurospheres in the presence and absence of doxycycline, the number of neurosphere cells was not significantly different 1 week after passage, regardless of doxycycline exposure (Fig. 3B). By contrast, the number of cells constituting the neurospheres exposed to doxycycline was significantly decreased after long-term culture of the neurospheres (Fig. 3C), suggesting that the ablation of *Rest* inhibited the growth of the neurospheres. Since a recent study demonstrated that *Rest* ablation in cultured neurosphere cells actually results in decreased proliferation (Gao et al., 2011), the decreased proliferative activity might be responsible for the decreased number of cultured cells upon doxycycline treatment in vitro.

We next cultured *Rest* conditional KO neurospheres (*Rest*$^{2lox/2lox}$; *Rosa26::rtTA*; *Col1a1::tetO-Cre*) under differentiation conditions. To examine the effects of *Rest* ablation on neuronal differentiation, the

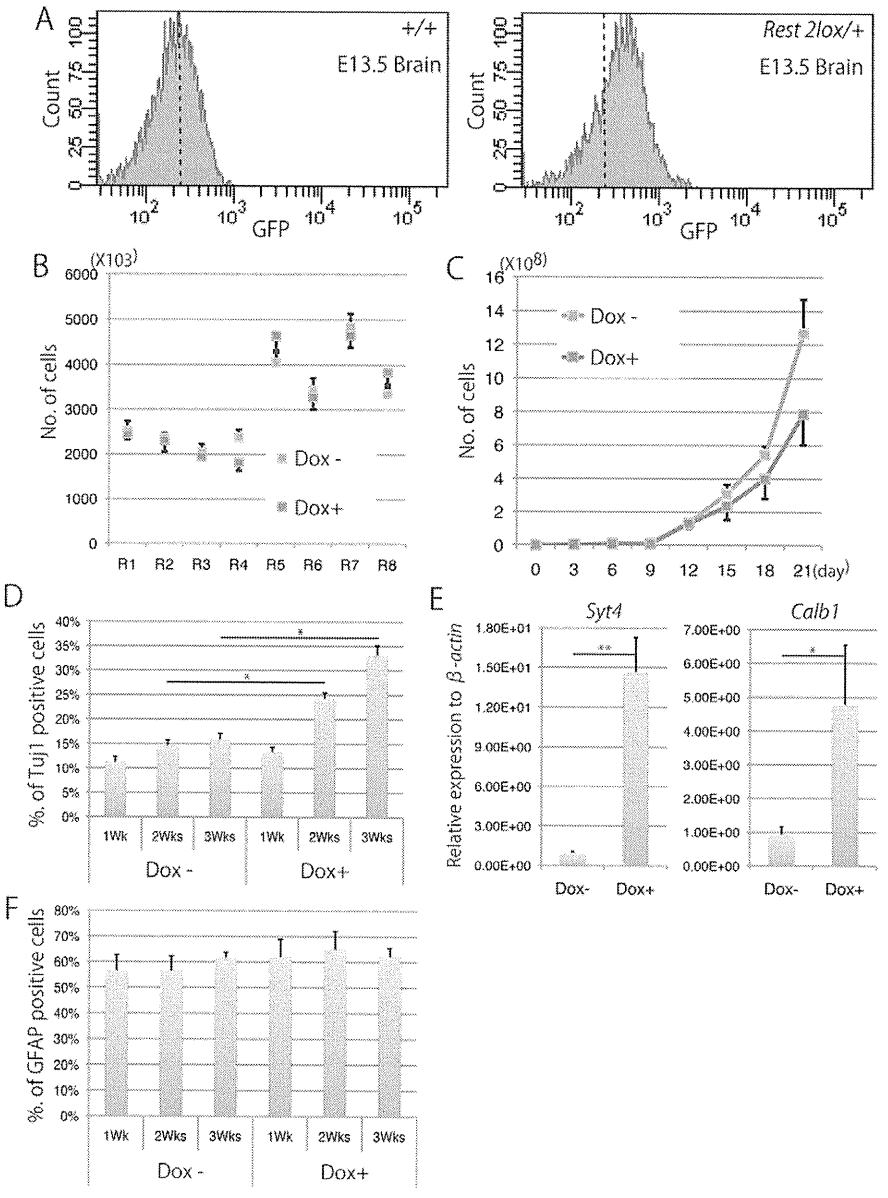

Fig. 3. *Rest* ablation in in vitro cultured neuronal cells. (**A**) FACS analysis for GFP fluorescence. The $Rest^{2lox}$ allele contains IRES-GFP sequences at the 3′UTR of the *Rest* gene, which allows visualization of *Rest* expression via GFP signals. Cells in the E13.5 mouse brain expressed GFP, suggesting that *Rest* is expressed in the developing brain. Dashed line represents the GFP signal at the peak of the histogram of the control cells for comparison. (**B**) The number of neurosphere cells in the presence and absence of doxycycline. The data are presented as the mean number of neurosphere cells in eight independent experiments (R1-R8). Error bars indicate s.d. (**C**) The number of cells constituting neurospheres in the presence and absence of doxycycline. Doxycycline-treated neurospheres grew more slowly than control neurospheres. Error bars indicate s.d. (**D**) The percentage of Tuj1-positive cells among total differentiated neurosphere cells after genetic deletion of *Rest*. The number of Tuj1-positive cells among total cells was significantly increased after *Rest* ablation. The data are presented as average values with s.d. of three independent samples. (**E**) The expression of *Syt4* and *Calb1* is derepressed after *Rest* ablation in neurosphere-derived differentiated cells. Transcript levels were normalized to β-actin levels. The data are presented as average values with s.d. of six independent samples. (**F**) The percentage of Gfap-positive cells among total differentiated neurosphere cells after genetic deletion of *Rest*. The number of Gfap-positive cells among total cells did not change following genetic ablation of *Rest*. The data are presented as average values with s.d. of three independent samples. *, $P<0.001$; **, $P<0.00005$.

doxycycline treatment was started 1 day after seeding the neurospheres in adherent culture, and the cells were treated with doxycycline for an additional 3 days. The adherent spheres were stained with anti-Tuj1 and anti-Gfap antibodies 1, 2 and 3 weeks after doxycycline exposure (Fig. 3D and supplementary material Fig. S5) and we counted the number of Tuj1-positive or Gfap-positive cells and DAPI-positive (total) nuclei in three independent areas of 1.5 mm^2 to calculate the proportion of Tuj1-positive or Gfap-positive cells. The doxycycline-treated cells contained a significantly increased percentage of Tuj1-positive cells among total cells than the control non-treated cells after 2 and 3 weeks of the treatment (Fig. 3D). In addition, a real-time PCR analysis revealed that the expression levels of *Syt4* and *Calb1* increased in the neurosphere adherent culture after genetic ablation of *Rest* (Fig. 3E). By contrast, the percentage of Gfap-positive glial cells among total cells was not altered (Fig. 3F), suggesting that ablation of *Rest* does not have a significant effect on glial differentiation in vitro in this experimental condition.

Because the Tuj1 and Gfap double-negative cells in the adherent spheres decreased after doxycycline treatment, *Rest* ablation may induce Tuj1 expression in such Tuj1 and Gfap double-negative cells. Immunocytochemical analysis of doxycycline-treated neurosphere cells revealed that a subset of non-neuron-like cells expresses Tuj1 and/or calbindin, whereas non-neuron-like cells in the control neurospheres did not express these markers (supplementary material Fig. S6A,B). Consistent with a previous study (Gao et al., 2011), we observed a small number of cells that express both Tuj1 and Gfap, suggesting the misexpression of Rest target genes (supplementary material Fig. S6C). Collectively, these results suggest that derepression of Rest target genes occurred in the adherent neurosphere cells upon *Rest* ablation, and that this derepression might play a role in the promotion of neuronal differentiation.

The in vivo effects of *Rest* ablation on gene expressions in non-neuronal and neuronal cells of the developing embryo

In the E13.5 mouse embryo the expression level of *Rest* in the limb was higher than that in the brain (supplementary material Fig. S7). By contrast, the expression level of Rest target genes was higher in the brain than in the limb (supplementary material Fig. S7).

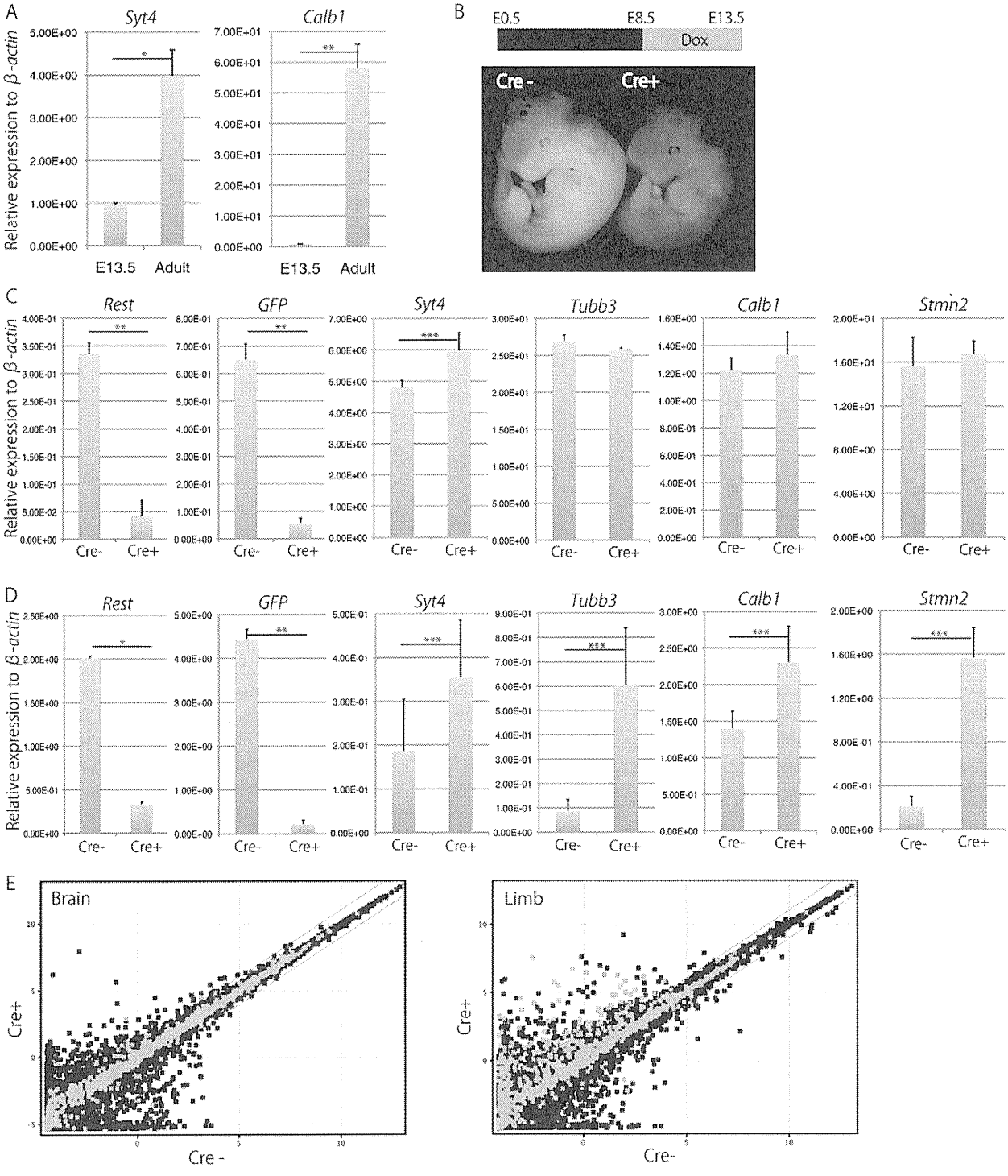

Fig. 4. In vivo genetic ablation of *Rest* in developing embryos. (**A**) Neuronal gene expression levels in the brains of E13.5 embryos and adult mice. The expression of *Syt4* and *Calb1* was significantly higher in the adult brain, suggesting that Rest neuronal target genes are still repressed in the E13.5 brain. The transcript levels were normalized to β-actin. The data are presented as average values with s.d. of six independent samples. (**B**) The experimental protocol for recombination of the *Rest* alleles in vivo. Pregnant mice with *Rest* conditional KO embryos were treated with doxycycline for 5 days, and embryos were sacrificed at E13.5. GFP fluorescence was decreased in embryos with the *tetO-Cre* allele, as compared with control embryos without the *tetO-Cre* allele. (**C**) The in vivo expression of Rest target genes in the brain. Although the expression levels of *Rest* and *GFP* were significantly downregulated, the expression levels of most Rest target genes were not derepressed in the brains of *Cre*+ embryos. Transcript levels were normalized to β-actin. The data are presented as average values with s.d. of four independent samples. (**D**) The expression of Rest target genes in the peripheral tissues (limb) in vivo. The expression of *Syt4*, *Tubb3*, *Calb1* and *Stmn2* was derepressed after genetic deletion of *Rest*. Transcript levels were normalized to β-actin. The data are presented as average values with s.d. of four independent samples. (**E**) A microarray analysis of E13.5 brain and non-neuronal (limb) tissue after genetic ablation of *Rest*. Rest binding genes in neuronal stem cells (Johnson et al., 2008) are shown as green dots. Rest target genes were significantly upregulated in the *Rest*-deleted non-neuronal tissue (limb). By contrast, the derepression of Rest target genes in the brain was not observed following genetic ablation of *Rest*. *, $P<0.01$; **, $P<0.005$; ***, $P<0.05$.

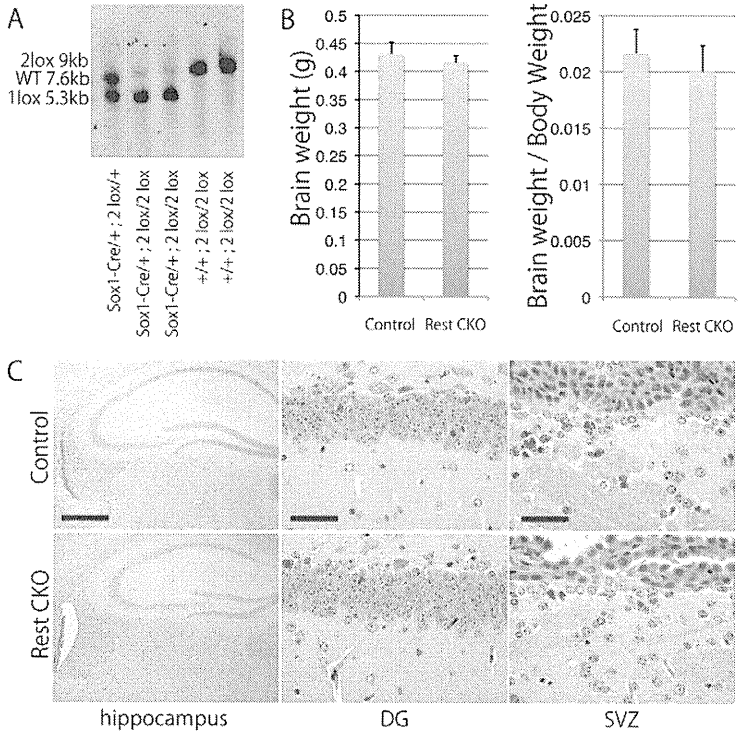

Fig. 5. The effect of *Rest* ablation on neurogenesis in vivo. (**A**) Southern blot analysis revealed that *Rest* conditional KO (2lox, 9kb) alleles in the adult brain with the *Sox1-Cre* allele recombined to form KO (1lox, 5.3kb) alleles. The wild-type (WT) allele appeared at 7.6 kb. (**B**) Comparison of brain weight and the ratio of brain weight to body weight in 8-week-old *Rest* conditional KO and control mice. Neither the brain weight nor the ratio was significantly different in *Sox1-Cre/+*; $Rest^{2lox/2lox}$ adult mice compared with control littermates. (**C**) The histology of adult brains from *Sox1-Cre/+*; $Rest^{2lox/2lox}$ mice (8 weeks of age). No histological differences were detectable in the dentate gyrus (DG, middle) of the hippocampus (left) and subventricular zone (SVZ, right) of the brains from *Sox1-Cre/+*; $Rest^{2lox/2lox}$ versus control adult mice by HE staining. Scale bars: 50 μm in DG and SVZ; 500 μm in hippocampus.

However, the expression levels of *Syt4* and *Calb1* in the E13.5 brain were significantly lower than those in the adult brain (Fig. 4A). These observations are consistent with the hypothesis that the expression of Rest target genes is still repressed in the E13.5 brain in vivo. Since our in vitro experiments revealed that the genetic ablation of *Rest* results in the increased expression of Rest target genes in both non-neuronal and neuronal cells, we next tried to dissect the effects of *Rest* ablation on the non-neuronal and neuronal cells in vivo using embryos with floxed *Rest* genes and doxycycline-inducible *Cre* alleles. The *Rest* conditional KO embryos were treated with doxycycline in utero (E8.5-13.5) to induce Cre-mediated recombination in both non-neuronal and neuronal cells, and the mice were sacrificed at E13.5 (Fig. 4B). In accordance with the recombination, E13.5 embryos with a *tetO-Cre* allele had decreased signals for GFP when compared with embryos without a *tetO-Cre* allele (Fig. 4B). We also collected the brains and limbs from *Rest*-deleted embryos and their control littermates without the *tetO-Cre* allele. Consistent with the decreased GFP signals, real-time RT-PCR analysis revealed that the expression of *Rest* was significantly downregulated in both the brain and limbs from embryos with a *tetO-Cre* allele compared with those from control littermates (Fig. 4C,D).

Similar to the results obtained in vitro, we detected a significant increase in the expression of *Syt4*, *Tubb3*, *Calb1* and *Stmn2* in the limbs of embryos with the *tetO-Cre* allele (Fig. 4D). By contrast, the expression level of *Tubb3*, *Calb1* and *Stmn2* in the brains of E13.5 embryos with a *tetO-Cre* allele remained repressed, whereas the expression levels of *Rest* and *GFP* itself were downregulated in the same samples (Fig. 4C). Although the expression of *Syt4* was slightly upregulated in the brain of embryos with a *tetO-Cre* allele (Fig. 4C), the effect was only modest when compared with the levels in the adult brain (Fig. 4A). Immunohistochemical analysis confirmed that there was no alteration in the expression pattern of Tuj1 in the E13.5 brain of embryos with a *tetO-Cre* allele (supplementary material Fig. S8A). We also examined the expression of Rest target genes in the brain or tail of E16.5 embryos with a *tetO-Cre* allele, and found no altered expression levels of these genes in brains, whereas a significant increase in the expression of *Syt4*, *Calb1* and *Stmn2* was observed in the tail (supplementary material Fig. S8B). These results indicate that the Rest target genes are specifically derepressed in non-neuronal cells outside of the brain by the genetic ablation of *Rest* in vivo.

We next performed a microarray analysis to determine the changes in gene expression after genetic deletion of *Rest* in E13.5 brain and limb in vivo. Consistent with the results of the real-time RT-PCR analysis, Rest target genes were significantly upregulated in the *Rest*-deleted limb tissue (Fig. 4E; genes interacting with Rest in ESCs and NPCs are represented by green dots) (Johnson et al., 2008). However, the derepression in the limb tissues (upregulated more than 2-fold after *Rest* ablation) was observed in only a subset of the genes with a Rest binding site (27% of the genes; Fig. 4E, limb), suggesting gene-specific derepression. By contrast, only 2% of the genes with a Rest binding site were upregulated more than 2-fold in the brain, suggesting that the derepression only occurs at a minority of Rest target genes after the genetic ablation of *Rest* (Fig. 4E, brain).

In vivo ablation of *Rest* in progenitor cells of the developing brain

Sox1 was shown to be one of the earliest transcription factors expressed in ectoderm cells committed to a neural fate (Pevny et al., 1998; Takashima et al., 2007). The expression of *Sox1* starts at E7.5-8.5 in the neural tube (Takashima et al., 2007). We used a *Sox1-Cre* allele (Takashima et al., 2007) ($Rest^{2lox/2lox}$; *Sox1-Cre/+*) to excise the floxed *Rest* genes in early progenitor cells of the developing mouse brain in vivo. The brains from *Rest* conditional KO mice carrying the *Sox1-Cre* allele ($Rest^{2lox/2lox}$; *Sox1-Cre/+*) and control littermates ($Rest2^{lox/2lox}$) were collected at E13.5, E16.5 and postnatal day (P) 0 and the expression levels of Rest target genes were compared by real-time RT-PCR. The brains from

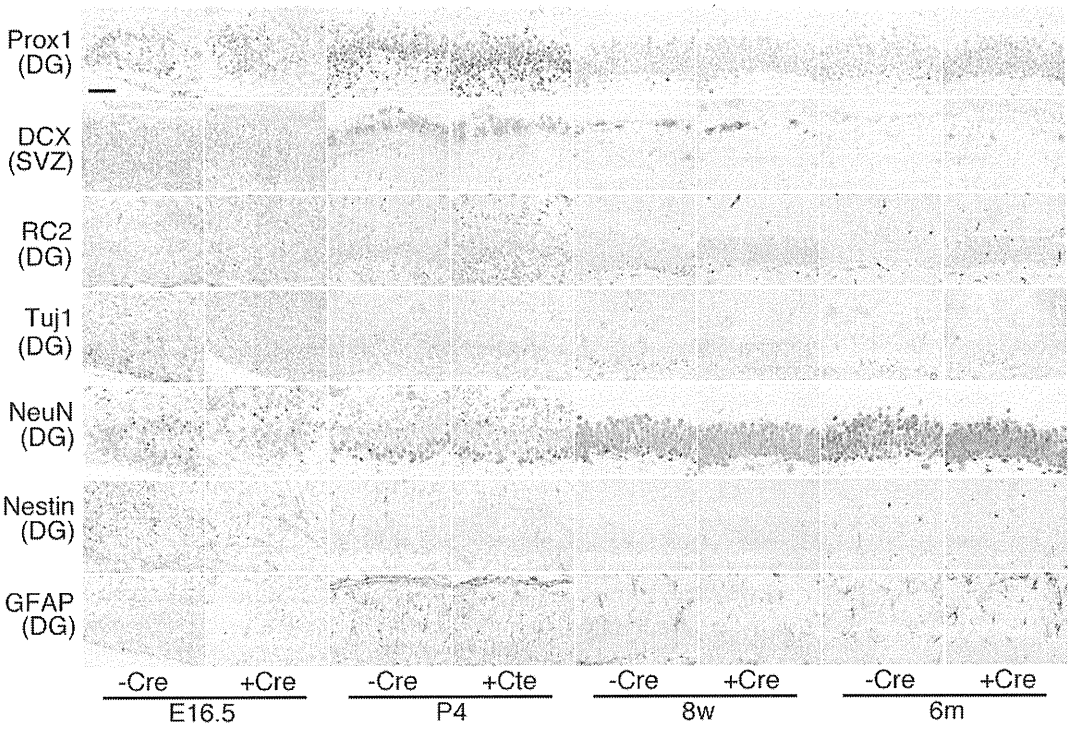

Fig. 6. Sequential immunohistochemical analysis for Prox1, Dcx, RC2, Tuj1, NeuN, nestin and Gfap. Brains at E16.5, P4, 8 weeks (8w) and 6 months (6m) of *Rest*-deficient and control mice were analyzed. DG, dentate gyrus; SVZ, subventricular zone. Scale bar: 50 μm.

embryos carrying *Sox1-Cre* had significantly lower levels of both *Rest* and *GFP* expression at all time points, reflecting the genetic ablation of *Rest* (supplementary material Fig. S9). However, consistent with the results in the experiments using doxycycline-inducible *Cre* mice, the expression levels of Rest target genes such as *Syt4*, *Tubb3*, *Calb1*, *Bdnf* and *Stmn2* (except for *Stmn2* at E13.5) were not significantly increased in the brains of developing embryos with the *Sox1-Cre* allele (supplementary material Fig. S9). These results confirm that the conditional deletion of *Rest* does not substantially affect the expression of Rest neuronal target genes in the developing brain.

Rest ablation during adult neurogenesis in vivo

To further examine the function of *Rest* in the maintenance of neurogenesis in adult brain tissue, we analyzed the brains of adult *Rest* conditional KO mice carrying the *Sox1-Cre* allele. Contrary to our expectation, the *Rest* conditional KO mice carrying the *Sox1-Cre* allele were apparently normal and grew into adults. These mice were viable for more than 1.5 years and were fertile. A Southern blot analysis confirmed that the brains of mice with the *Sox1-Cre* allele had lost the floxed *Rest* genes (Fig. 5A). Despite the lack of *Rest* throughout the entire brain tissue (Fig. 5A), brain weight at 8 weeks of age was not significantly different between the mice with and without the *Sox1-Cre* allele (Fig. 5B).

Next, we examined the histology of the brains of mice with and without the *Sox1-Cre* allele at different developmental stages and ages (E16.5, P0, P4, P7, P10, 4 weeks, 8 weeks, 10 weeks, 6 months and 9 months of age). However, we did not find any histological differences in the brains, including in the subgranular zone (SGZ) of the hippocampal dentate gyrus and the subventricular zone (SVZ), where NSCs and NPCs reside and generate new neurons and glia (Fig. 5C) (Gage, 2002). We further performed immunohistochemical staining to examine the expression of various markers, including Prox1, Dcx, RC2, Tuj1, NeuN (Rbfox3 – Mouse Genome Informatics), nestin and Gfap at various time points (E16.5, P4, 8 weeks and 6 months) in the *Rest*-deficient and control brains. Prox1, Dcx and RC2 were used as markers for intermediate progenitor cells, immature neuronal cells and radial glial cells, respectively (Gao et al., 2011; Misson et al., 1988). Importantly, we did not observe any difference in the staining patterns of these markers between *Rest*-deficient and control brains (Fig. 6). We also confirmed that nestin-positive cells and Gfap-positive cells did not express Tuj1 in *Rest*-deficient brain, suggesting that misexpression of Tuj1 does not occur in the *Rest*-deficient cells in vivo (supplementary material Figs S10, S11). Although a recent study showed that acute *Rest* ablation in mice leads to a decreased number of Prox1-positive cells at SGZ regions, we did not observe any significant differences in the number of Prox1-positive cells, even in 9-month-old mice (supplementary material Fig. S12).

In order to examine the effect of *Rest* ablation on the maintenance of adult NSCs, we compared the numbers of BrdU-labeled cells in the SVZ of the adult brain of the *Rest* conditional KO mice carrying the *Sox1-Cre* allele with those of control littermates (Doetsch et al., 2002; Lendahl et al., 1990). BrdU was administered as a daily intraperitoneal injection of 50 mg/kg body weight for 12 days starting at the age of 8 weeks, and the brains were fixed 1 day after the last injection as described previously (Shi et al., 2004). We did not find any significant difference in the number of BrdU-positive cells in the SVZ of these mice (Fig. 7A). We also confirmed co-localization of BrdU-positive cells and those positive for Dcx, a marker for premature neuronal cells, in the SVZ of *Rest*-deficient mice (Fig. 7B), suggesting that adult neurogenesis occurs in these mice. In addition, the localization and the number of differentiated NeuN-positive cells in the adult mouse brain did not differ in the presence or absence of the intact *Rest* gene (Fig.

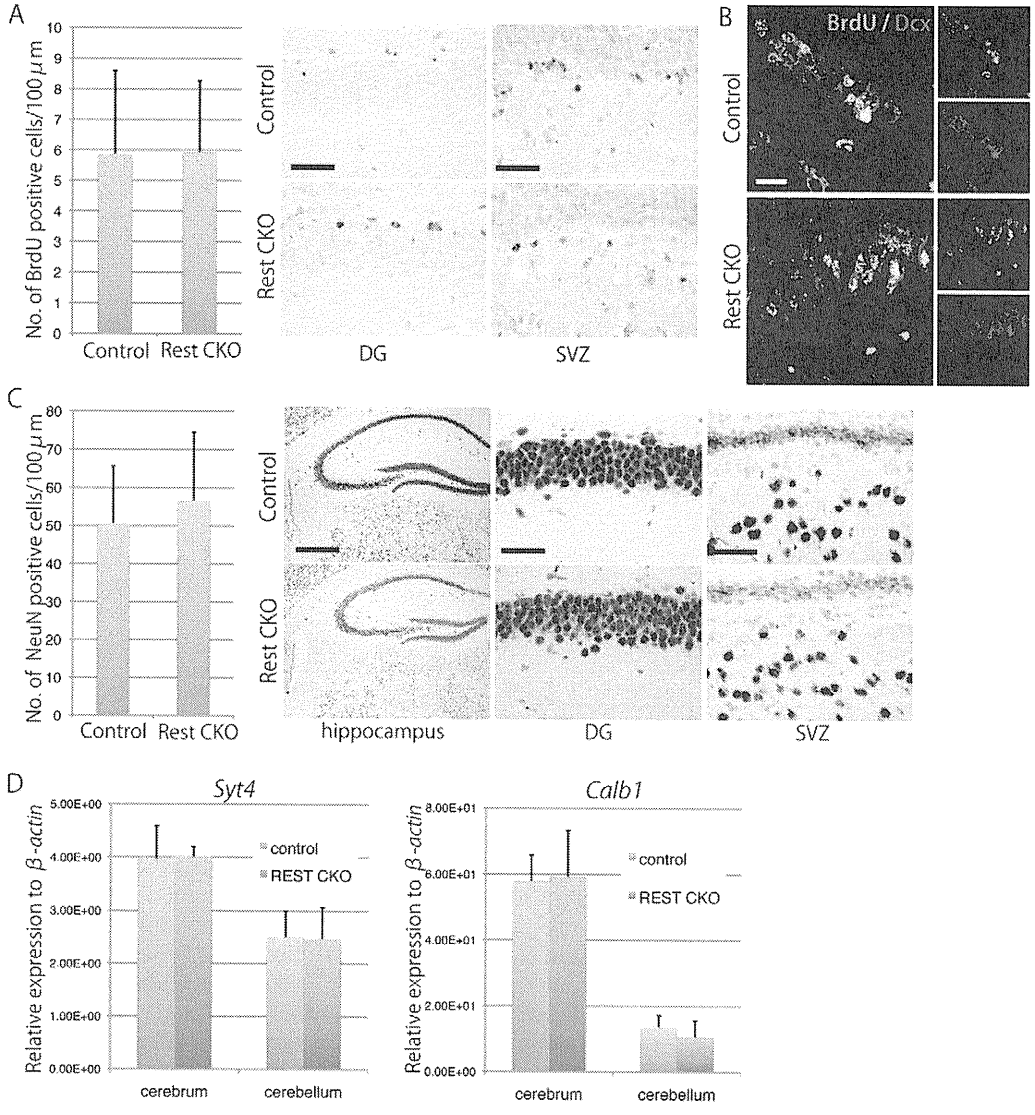

Fig. 7. Adult neurogenesis in *Rest*-deficient brains in vivo. (**A**) Immunohistochemical analysis of BrdU-positive proliferating cells in the adult brain (10 weeks of age). There were no differences in the distribution of BrdU-positive cells in DG and SVZ regardless of genotype. The number of BrdU-positive cells/length of cerebral ventricle in the brains of *Sox1-Cre/+*; *Rest*$^{2lox/2lox}$ mice was not altered compared with that of their control littermates. (**B**) Immunohistochemical staining for BrdU (green) and Dcx (red) double-positive cells in the SVZ of brain from *Sox1-Cre/+*; *Rest*$^{2lox/2lox}$ mice and control littermates at 10 weeks of age. (**C**) Immunohistochemical staining for NeuN in the DG of the hippocampus and SVZ of brains from *Sox1-Cre/+*; *Rest*$^{2lox/2lox}$ mice and their control littermates at 8 weeks of age. (**D**) The expression of Rest target genes in the adult mouse brain at 8 weeks of age. The expression of *Syt4* and *Calb1* was unchanged in the cerebrum and cerebellum of *Sox1-Cre/+*; *Rest*$^{2lox/2lox}$ mice. Transcript levels were normalized to β-actin levels. The data are presented as average values with s.d. of six independent samples. Scale bars: 50 μm in DG and SVZ; 500 μm in hippocampus; 20 μm in B.

7C). A real-time RT-PCR analysis revealed that the expression of *Syt4* and *Calb1* was not altered in the adult brains lacking the CoRest binding site of *Rest* (Fig. 7D).

These results indicate that *Rest* is not required for brain development and suggest that genetic ablation of *Rest* during the initial stage of neural development does not cause any detectable abnormality in adult neurogenesis in vivo.

DISCUSSION

Differentiation of neuronal progenitors to mature neurons proceeds with loss of the Rest repressor complex from the RE1 site of neuronal genes, which is accompanied by increased expression of the target genes (Ballas et al., 2005). In the present study, using *Rest* conditional KO mice we confirmed that *Rest* plays a role in the repression of Rest neuronal target genes in in vitro cultured neuronal progenitor cells to inhibit terminal differentiation. By contrast, genetic ablation of *Rest* in the whole brain in vivo does not result in altered expression of target genes. Furthermore, mice lacking *Rest* in the brain are apparently normal and grow into adults. These findings suggest that, in contrast to the repressive role of *Rest* in in vitro cultured neuronal cells, *Rest* is dispensable for embryonic neurogenesis in vivo.

The unsolved question is why derepression of Rest target genes after *Rest* ablation can be detected in in vitro cultured neuronal cells but not in developing brain tissue in vivo. It has been demonstrated that neuronal progenitor cells are competent for extrinsic signals involved in the specification of cell fate during neurogenesis (Edlund and Jessell, 1999). Our findings suggest that the local environment in the brain, which consists of multiple cell types, is likely to provide complementary regulatory mechanisms for the proper intrinsic regulation of neuronal genes in vivo. It is noteworthy that, in the non-neuronal cells outside of the brain, the derepression of Rest target genes was observed not only in vitro but also in vivo. These findings suggest that the brain-specific environment is important for the complementary repression of Rest target genes in the absence of *Rest*.

Epigenetic mechanisms serve as important interfaces between gene expression and the environment (Jaenisch and Bird, 2003). Given that Rest exerts its repressive effects in conjunction with epigenetic modifiers (Ballas et al., 2005; Naruse et al., 1999; You et al., 2001), it is possible that extrinsic niche signals in the brain compensate for the lack of Rest through epigenetic regulatory mechanisms. Consistent with this hypothesis, we could not detect

any differences in the staining pattern of histone H3K27me3, a mark of epigenetic silencing, between *Rest* wild-type and *Rest*-deficient brains in vivo (data not shown).

Another study indicated that MeCP2 and other co-repressors remained on the Rest target promoters even after loss of Rest from the RE1 site, suggesting that Rest co-repressors might be involved in the additional regulatory mechanisms that are responsible for repressing the expression of neuronal genes in neuronal cells in the absence of Rest (Ballas et al., 2005). It is possible that such factors specifically compensate for the effect of *Rest* ablation in the repression of Rest neuronal target genes during embryonic neurogenesis in vivo. It is also possible that transcriptional activators might be required for the derepression of Rest target genes in the developing brain. In this context, the decreased levels of transcriptional activation might maintain the proper expression levels of Rest target genes in *Rest*-deficient brains in vivo.

A recent study by Gao et al. demonstrated that the acute deletion of *Rest* in the adult dentate gyrus (DG) leads to a decreased number of Prox1-positive DG cells (Gao et al., 2011). However, in the present study, we did not observe any significant differences in the number of Prox1-positive DG cells upon *Rest* ablation, even in 9-month-old mice. A possible explanation for the discrepancy is that the acute deletion of *Rest* in the adult DG cannot activate the compensatory mechanisms, resulting in premature differentiation of adult NSCs, whereas its deletion at the early embryonic stage, as performed in this experiment, activates the complementary machinery that masks Rest function at adult stages. Therefore, further experiments are still required to determine the role of Rest in the maintenance of adult NSCs in vivo.

The expression of Rest target genes in MEFs/TTFs is upregulated upon the loss of *Rest*, suggesting that Rest is involved in the active repression of neuronal genes in non-neuronal cells outside of the brain. However, we found that *Bdnf*, which contains RE1 sites and is repressed by Rest in ESCs (Yamada et al., 2010), was not derepressed after the deletion of *Rest* in MEFs/TTFs. As reported in a previous study (Chen et al., 1998), these findings suggest that there is cell type specificity of Rest-mediated gene silencing. In addition, a microarray analysis revealed that only a subset of genes with a Rest binding site (27%) is derepressed by more than 2-fold following genetic ablation of *Rest* in non-neuronal tissues. In addition to the cell type-specific repression, these findings suggest that there is gene-specific repression by Rest (Chen et al., 1998). Since epigenetic silencing occurs through multiple modifications, including DNA methylation and histone modifications (Jaenisch and Bird, 2003; Lunyak et al., 2002; Martinowich et al., 2003), *Rest* deletion alone might not be sufficient to reactivate the silenced locus once silencing, involving multiple epigenetic modifications, has been completed. It is also possible that the cell type- and gene-specific activity of transcriptional activators is responsible for such different responses to *Rest* deletion.

The impaired interaction of Rest with its target genes has been reported in various neurological and neurodegenerative diseases. Although we found that mice lacking the CoRest binding site of *Rest* in the brain had no gross anatomical abnormalities even upon reaching adulthood, it is possible that more detailed analyses might highlight behavioral abnormalities in the *Rest* KO mice. In this context, these mice might be useful in investigation of the role of altered Rest interactions in neurological and neurodegenerative diseases. It would also be interesting to examine the functional alterations of *Rest*-deficient neuronal cells in vivo, which eventually might uncover the pathogenesis of such diseases.

In summary, we have generated *Rest* conditional KO mice and examined the effects of *Rest* ablation in neuronal and non-neuronal cells in vitro and in vivo. We showed that, in contrast to the role of *Rest* in the repression of Rest target genes in in vitro cultured neuronal cells, as well as in non-neuronal cells outside of the brain, the CoRest binding site of *Rest* is dispensable for embryonic neurogenesis in vivo.

Acknowledgements
We thank Kyoko Takahashi and Ayako Suga for technical assistance; Caroline Beard for the *Col1a-tetOP-cre* allele; and Shinichi Nishikawa for *Sox1-Cre* mice.

Funding
This study was supported by grants from the Ministry of Education, Culture, Sports, Science and Technology of Japan; Precursory Research for Embryonic Science and Technology (PRESTO); and the Ministry of Health, Labour and Welfare of Japan.

Competing interests statement
The authors declare no competing financial interests.

Supplementary material
Supplementary material available online at
http://dev.biologists.org/lookup/suppl/doi:10.1242/dev.072272/-/DC1

References

Abrajano, J. J., Qureshi, I. A., Gokhan, S., Zheng, D., Bergman, A. and Mehler, M. F. (2009). Differential deployment of REST and CoREST promotes glial subtype specification and oligodendrocyte lineage maturation. *PLoS ONE* **4**, e7665.

Andres, M. E., Burger, C., Peral-Rubio, M. J., Battaglioli, E., Anderson, M. E., Grimes, J., Dallman, J., Ballas, N. and Mandel, G. (1999). CoREST: a functional corepressor required for regulation of neural-specific gene expression. *Proc. Natl. Acad. Sci. USA* **96**, 9873-9878.

Ballas, N., Battaglioli, E., Atouf, F., Andres, M. E., Chenoweth, J., Anderson, M. E., Burger, C., Moniwa, M., Davie, J. R., Bowers, W. J. et al. (2001). Regulation of neuronal traits by a novel transcriptional complex. *Neuron* **31**, 353-365.

Ballas, N., Grunseich, C., Lu, D. D., Speh, J. C. and Mandel, G. (2005). REST and its corepressors mediate plasticity of neuronal gene chromatin throughout neurogenesis. *Cell* **121**, 645-657.

Bassuk, A. G., Wallace, R. H., Buhr, A., Buller, A. R., Afawi, Z., Shimojo, M., Miyata, S., Chen, S., Gonzalez-Alegre, P., Griesbach, H. L. et al. (2008). A homozygous mutation in human PRICKLE1 causes an autosomal-recessive progressive myoclonus epilepsy-ataxia syndrome. *Am. J. Hum. Genet.* **83**, 572-581.

Beard, C., Hochedlinger, K., Plath, K., Wutz, A. and Jaenisch, R. (2006). Efficient method to generate single-copy transgenic mice by site-specific integration in embryonic stem cells. *Genesis* **44**, 23-28.

Bruce, A. W., Donaldson, I. J., Wood, I. C., Yerbury, S. A., Sadowski, M. I., Chapman, M., Gottgens, B. and Buckley, N. J. (2004). Genome-wide analysis of repressor element 1 silencing transcription factor/neuron-restrictive silencing factor (REST/NRSF) target genes. *Proc. Natl. Acad. Sci. USA* **101**, 10458-10463.

Canzonetta, C., Mulligan, C., Deutsch, S., Ruf, S., O'Doherty, A., Lyle, R., Borel, C., Lin-Marq, N., Delom, F., Groet, J. et al. (2008). DYRK1A-dosage imbalance perturbs NRSF/REST levels, deregulating pluripotency and embryonic stem cell fate in Down syndrome. *Am. J. Hum. Genet.* **83**, 388-400.

Chen, Z. F., Paquette, A. J. and Anderson, D. J. (1998). NRSF/REST is required in vivo for repression of multiple neuronal target genes during embryogenesis. *Nat. Genet.* **20**, 136-142.

Chong, J. A., Tapia-Ramirez, J., Kim, S., Toledo-Aral, J. J., Zheng, Y., Boutros, M. C., Altshuller, Y. M., Frohman, M. A., Kraner, S. D. and Mandel, G. (1995). REST: a mammalian silencer protein that restricts sodium channel gene expression to neurons. *Cell* **80**, 949-957.

Doetsch, F., Petreanu, L., Caille, I., Garcia-Verdugo, J. M. and Alvarez-Buylla, A. (2002). EGF converts transit-amplifying neurogenic precursors in the adult brain into multipotent stem cells. *Neuron* **36**, 1021-1034.

Edlund, T. and Jessell, T. M. (1999). Progression from extrinsic to intrinsic signaling in cell fate specification: a view from the nervous system. *Cell* **96**, 211-224.

Fink, T. L., Francis, S. H., Beasley, A., Grimes, K. A. and Corbin, J. D. (1999). Expression of an active, monomeric catalytic domain of the cGMP-binding cGMP-specific phosphodiesterase (PDE5). *J. Biol. Chem.* **274**, 34613-34620.

Gage, F. H. (2002). Neurogenesis in the adult brain. *J. Neurosci.* **22**, 612-613.

Gao, Z., Ure, K., Ding, P., Nashaat, M., Yuan, L., Ma, J., Hammer, R. E. and Hsieh, J. (2011). The master negative regulator REST/NRSF controls adult

neurogenesis by restraining the neurogenic program in quiescent stem cells. *J. Neurosci.* **31**, 9772-9786.

Hatano, Y., Yamada, Y., Hata, K., Phutthaphadoong, S., Aoki, H. and Hara, A. (2011). Genetic ablation of a candidate tumor suppressor gene, Rest, does not promote mouse colon carcinogenesis. *Cancer Sci.* **102**, 1659-1664.

Hochedlinger, K., Yamada, Y., Beard, C. and Jaenisch, R. (2005). Ectopic expression of Oct-4 blocks progenitor-cell differentiation and causes dysplasia in epithelial tissues. *Cell* **121**, 465-477.

Jaenisch, R. and Bird, A. (2003). Epigenetic regulation of gene expression: how the genome integrates intrinsic and environmental signals. *Nat. Genet.* **33 Suppl.**, 245-254.

Jepsen, K., Hermanson, O., Onami, T. M., Gleiberman, A. S., Lunyak, V., McEvilly, R. J., Kurokawa, R., Kumar, V., Liu, F., Seto, E. et al. (2000). Combinatorial roles of the nuclear receptor corepressor in transcription and development. *Cell* **102**, 753-763.

Johnson, R., Gamblin, R. J., Ooi, L., Bruce, A. W., Donaldson, I. J., Westhead, D. R., Wood, I. C., Jackson, R. M. and Buckley, N. J. (2006). Identification of the REST regulon reveals extensive transposable element-mediated binding site duplication. *Nucleic Acids Res.* **34**, 3862-3877.

Johnson, R., Teh, C. H., Kunarso, G., Wong, K. Y., Srinivasan, G., Cooper, M. L., Volta, M., Chan, S. S., Lipovich, L., Pollard, S. M. et al. (2008). REST regulates distinct transcriptional networks in embryonic and neural stem cells. *PLoS Biol.* **6**, e256.

Kohyama, J., Sanosaka, T., Tokunaga, A., Takatsuka, E., Tsujimura, K., Okano, H. and Nakashima, K. (2010). BMP-induced REST regulates the establishment and maintenance of astrocytic identity. *J. Cell Biol.* **189**, 159-170.

Lendahl, U., Zimmerman, L. B. and McKay, R. D. (1990). CNS stem cells express a new class of intermediate filament protein. *Cell* **60**, 585-595.

Lepagnol-Bestel, A. M., Zvara, A., Maussion, G., Quignon, F., Ngimbous, B., Ramoz, N., Imbeaud, S., Loe-Mie, Y., Benihoud, K., Agier, N. et al. (2009). DYRK1A interacts with the REST/NRSF-SWI/SNF chromatin remodelling complex to deregulate gene clusters involved in the neuronal phenotypic traits of Down syndrome. *Hum. Mol. Genet.* **18**, 1405-1414.

Lunyak, V. V., Burgess, R., Prefontaine, G. G., Nelson, C., Sze, S. H., Chenoweth, J., Schwartz, P., Pevzner, P. A., Glass, C., Mandel, G. et al. (2002). Corepressor-dependent silencing of chromosomal regions encoding neuronal genes. *Science* **298**, 1747-1752.

Martinowich, K., Hattori, D., Wu, H., Fouse, S., He, F., Hu, Y., Fan, G. and Sun, Y. E. (2003). DNA methylation-related chromatin remodeling in activity-dependent BDNF gene regulation. *Science* **302**, 890-893.

Misson, J. P., Edwards, M. A., Yamamoto, M. and Caviness, V. S., Jr (1988). Identification of radial glial cells within the developing murine central nervous system: studies based upon a new immunohistochemical marker. *Brain Res. Dev. Brain Res.* **44**, 95-108.

Naruse, Y., Aoki, T., Kojima, T. and Mori, N. (1999). Neural restrictive silencer factor recruits mSin3 and histone deacetylase complex to repress neuron-specific target genes. *Proc. Natl. Acad. Sci. USA* **96**, 13691-13696.

Otto, S. J., McCorkle, S. R., Hover, J., Conaco, C., Han, J. J., Impey, S., Yochum, G. S., Dunn, J. J., Goodman, R. H. and Mandel, G. (2007). A new binding motif for the transcriptional repressor REST uncovers large gene networks devoted to neuronal functions. *J. Neurosci.* **27**, 6729-6739.

Pevny, L. H., Sockanathan, S., Placzek, M. and Lovell-Badge, R. (1998). A role for SOX1 in neural determination. *Development* **125**, 1967-1978.

Roopra, A., Qazi, R., Schoenike, B., Daley, T. J. and Morrison, J. F. (2004). Localized domains of G9a-mediated histone methylation are required for silencing of neuronal genes. *Mol. Cell* **14**, 727-738.

Schoenherr, C. J. and Anderson, D. J. (1995). The neuron-restrictive silencer factor (NRSF): a coordinate repressor of multiple neuron-specific genes. *Science* **267**, 1360-1363.

Schoenherr, C. J., Paquette, A. J. and Anderson, D. J. (1996). Identification of potential target genes for the neuron-restrictive silencer factor. *Proc. Natl. Acad. Sci. USA* **93**, 9881-9886.

Shi, Y., Sawada, J., Sui, G., Affar, El B., Whetstine, J. R., Lan, F., Ogawa, H., Luke, M. P. and Nakatani, Y. (2003). Coordinated histone modifications mediated by a CtBP co-repressor complex. *Nature* **422**, 735-738.

Shi, Y., Chichung Lie, D., Taupin, P., Nakashima, K., Ray, J., Yu, R. T., Gage, F. H. and Evans, R. M. (2004). Expression and function of orphan nuclear receptor TLX in adult neural stem cells. *Nature* **427**, 78-83.

Strutz, F., Okada, H., Lo, C. W., Danoff, T., Carone, R. L., Tomaszewski, J. E. and Neilson, E. G. (1995). Identification and characterization of a fibroblast marker: FSP1. *J. Cell Biol.* **130**, 393-405.

Takashima, Y., Era, T., Nakao, K., Kondo, S., Kasuga, M., Smith, A. G. and Nishikawa, S. (2007). Neuroepithelial cells supply an initial transient wave of MSC differentiation. *Cell* **129**, 1377-1388.

Tapia-Ramirez, J., Eggen, B. J., Peral-Rubio, M. J., Toledo-Aral, J. J. and Mandel, G. (1997). A single zinc finger motif in the silencing factor REST represses the neural-specific type II sodium channel promoter. *Proc. Natl. Acad. Sci. USA* **94**, 1177-1182.

Vierbuchen, T., Ostermeier, A., Pang, Z. P., Kokubu, Y., Sudhof, T. C. and Wernig, M. (2010). Direct conversion of fibroblasts to functional neurons by defined factors. *Nature* **463**, 1035-1041.

Yamada, Y., Aoki, H., Kunisada, T. and Hara, A. (2010). Rest promotes the early differentiation of mouse ESCs but is not required for their maintenance. *Cell Stem Cell* **6**, 10-15.

You, A., Tong, J. K., Grozinger, C. M. and Schreiber, S. L. (2001). CoREST is an integral component of the CoREST- human histone deacetylase complex. *Proc. Natl. Acad. Sci. USA* **98**, 1454-1458.

Zuccato, C., Belyaev, N., Conforti, P., Ooi, L., Tartari, M., Papadimou, E., MacDonald, M., Fossale, E., Zeitlin, S., Buckley, N. et al. (2007). Widespread disruption of repressor element-1 silencing transcription factor/neuron-restrictive silencer factor occupancy at its target genes in Huntington's disease. *J. Neurosci.* **27**, 6972-6983.

LETTER

doi:10.1038/nature10424

Targeted gene correction of α_1-antitrypsin deficiency in induced pluripotent stem cells

Kosuke Yusa[1]*, S. Tamir Rashid[2,3]*, Helene Strick-Marchand[4,5], Ignacio Varela[6], Pei-Qi Liu[7], David E. Paschon[7], Elena Miranda[3,8], Adriana Ordóñez[3], Nicholas R. F. Hannan[2], Foad J. Rouhani[1,2], Sylvie Darche[4,5], Graeme Alexander[9], Stefan J. Marciniak[3], Noemi Fusaki[10,11], Mamoru Hasegawa[10], Michael C. Holmes[7], James P. Di Santo[4,5], David A. Lomas[3]*, Allan Bradley[1]* & Ludovic Vallier[2]*

Human induced pluripotent stem cells (iPSCs) represent a unique opportunity for regenerative medicine because they offer the prospect of generating unlimited quantities of cells for autologous transplantation, with potential application in treatments for a broad range of disorders[1–4]. However, the use of human iPSCs in the context of genetically inherited human disease will require the correction of disease-causing mutations in a manner that is fully compatible with clinical applications[3,5]. The methods currently available, such as homologous recombination, lack the necessary efficiency and also leave residual sequences in the targeted genome[6]. Therefore, the development of new approaches to edit the mammalian genome is a prerequisite to delivering the clinical promise of human iPSCs. Here we show that a combination of zinc finger nucleases (ZFNs)[7] and *piggyBac*[8,9] technology in human iPSCs can achieve biallelic correction of a point mutation (Glu342Lys) in the α_1-antitrypsin (*A1AT*, also known as *SERPINA1*) gene that is responsible for α_1-antitrypsin deficiency. Genetic correction of human iPSCs restored the structure and function of A1AT in subsequently derived liver cells *in vitro* and *in vivo*. This approach is significantly more efficient than any other gene-targeting technology that is currently available and crucially prevents contamination of the host genome with residual non-human sequences. Our results provide the first proof of principle, to our knowledge, for the potential of combining human iPSCs with genetic correction to generate clinically relevant cells for autologous cell-based therapies.

At present, available methods for gene targeting rely on positive selection to isolate rare clones that have undergone homologous recombination. To remove the unwanted selection cassettes, Cre/*loxP* or Flp/*FRT* recombination systems are used, which leave behind single *loxP* or *FRT* sites[10,11]. These small ectopic sequences have the potential to interfere with transcriptional regulatory elements of surrounding genes[12], most of which are not fully characterized in the human genome. An alternative method to remove selection cassettes is to convert them into transposons. The most suitable transposon for this purpose is *piggyBac*, a moth-derived DNA transposon, which can transpose efficiently in mammalian cells including human embryonic stem (ES) cells[9,13]. A remarkable feature of this mobile element is seamless excision, which enables the removal of transgenes flanked by *piggyBac* inverted repeats without leaving any residual sequences[9,14].

To explore the use of *piggyBac* for the correction of point mutations, we designed a vector to correct an albino mutation (G290T substitution in the *Tyr* gene) in mouse iPSCs isolated from fibroblasts of the C57Bl6-*Tyr*$^{c\text{-}Brd}$ strain[15]. The targeting vector was constructed, carrying a wild-type 290G sequence and a *PGK-puroΔtk* cassette flanked by *piggyBac* repeats into the TTAA site (Fig. 1a). After isolation of targeted clones, the selection cassette was excised from the mouse iPSC genome by transient expression of the *piggyBac* transposase and subsequent 1-(2-deoxy-2-fluoro-β-D-arabinofuranosyl)-5-iodouracil

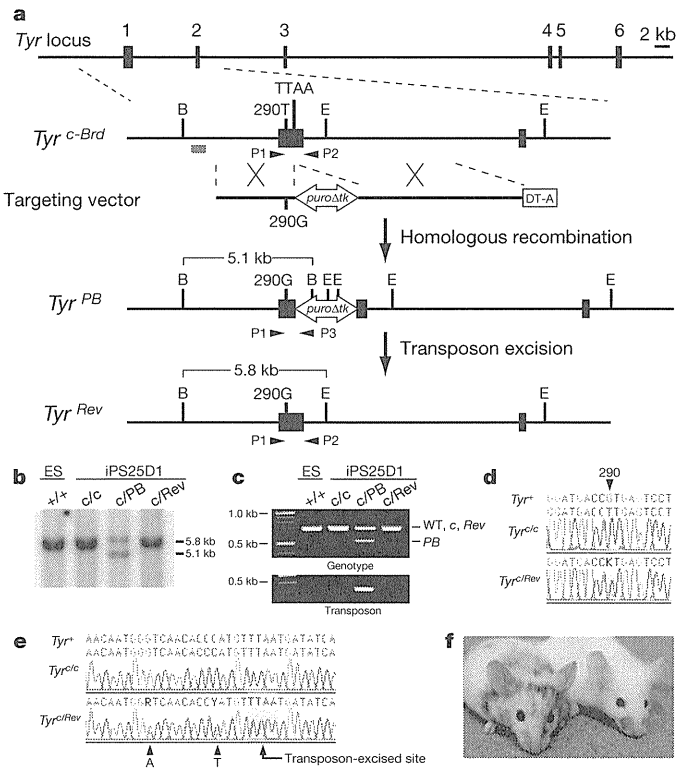

Figure 1 | Correction of the G290T mutation in the *Tyr* gene in mouse iPSCs. a, The strategy for precise genome modification using the *piggyBac* transposon. Top line, structure of the *Tyr* gene; red line, 5′ external probe for Southern blot analysis; open arrow, *piggyBac* transposon carrying a *PGK-puroΔtk* cassette; B, BamHI; E, EcoNI; P1, P2 and P3, PCR primers. **b**, **c**, Southern blot (**b**) and PCR analyses (**c**) showing insertion (c/PB) and excision (c/Rev) of the *piggyBac* transposon. ES, mouse ES cells as a control. **d**, **e**, Sequence analyses revealed correction of the G290T mutation (**d**) and seamless excision of the *piggyBac* transposon (**e**). Note that two silent mutations (A and T, indicated by arrowheads) introduced near the TTAA site were also detected. **f**, A chimaeric mouse generated by injecting corrected *Tyr*$^{c/Rev}$ mouse iPSCs (left) shows black coat colour. Right, a non-injected albino mouse.

[1]Wellcome Trust Sanger Institute, Wellcome Trust Genome Campus, Hinxton, Cambridge CB10 1SA, UK. [2]Anne McLaren Laboratory for Regenerative Medicine, Department of Surgery, West Forvie Building, Robinson Way, University of Cambridge, Cambridge CB2 0SZ, UK. [3]Department of Medicine, University of Cambridge, Cambridge Institute for Medical Research, Wellcome Trust/MRC Building, Hills Road, Cambridge CB0 2XY, UK. [4]Innate Immunity Unit, Institut Pasteur, 75724 Paris, France. [5]INSERM, U668, 75724 Paris, France. [6]Instituto de Biomedicina y Biotecnología de Cantabria (IBBTEC), CSIC-UC-SODERCAN Avda. Cardenal Herrera Oria s/n 39011 Santander, Spain. [7]Sangamo BioSciences Inc., Richmond, California 94804, USA. [8]Dept. Biologia e Biotecnologie 'Charles Darwin', Università di Roma "La Sapienza", p.le Aldo Moro 5, 00185 Rome, Italy. [9]Division of Gastroenterology and Hepatology, Department of Medicine, Cambridge University Hospitals NHS Trust, Cambridge CB2 2QQ, UK. [10]DNAVEC Corporation, Tsukuba, Ibaraki 300-2611, Japan. [11]PRESTO, JST, Saitama 332-0012, Japan.
*These authors contributed equally to this work.

(FIAU) selection. Genomic modification was verified by Southern blot and polymerase chain reaction (PCR) analyses (Fig. 1b, c). The correction of the G290T mutation and seamless *piggyBac* excision were confirmed by sequence analyses (Fig. 1d, e). Two introduced silent mutations were observed, confirming that the T290G substitution was mediated by gene correction, not by spontaneous reversion (Fig. 1e). The function of the reverted allele was tested by injecting the corrected mouse iPSCs into albino mouse blastocysts. The resulting chimaeric mice had a black coat colour, indicating phenotypic correction of the albino mutation (Fig. 1f). These results collectively demonstrate that the *piggyBac* transposon can be used as a versatile tool for highly precise modification (for example, correction or mutation) of the mammalian genome at a single base-pair level.

We next explored whether this approach could be used to correct a mutation in human iPSCs derived from individuals with α_1-antitrypsin deficiency (A1ATD)[16]. A1ATD is an autosomal recessive disorder found in 1 out of 2,000 individuals of North European descent and represents the most common inherited metabolic disease of the liver[17,18]. It results from a single point mutation in the *A1AT* gene (the *Z* allele; Glu342Lys) that causes the protein to form ordered polymers within the endoplasmic reticulum of hepatocytes[17,18]. The resulting inclusions cause cirrhosis for which the only current therapy is liver transplantation. The increasing shortage of donors and harmful effects of immunosuppressive treatments impose major limitations on organ transplantation, making the potential of human iPSC-based therapy highly attractive. Because homologous recombination is relatively inefficient in human ES cells[6] we used ZFN technology, which stimulates gene targeting in human ES cells as well as human iPSCs[7,10,19]. ZFN pairs were designed to specifically cleave the site of the *Z* mutation (Fig. 2a–c, Supplementary Table 1 and Supplementary Note). A targeting vector was constructed from isogenic DNA with *piggyBac* repeats flanking the *PGK-puroΔtk* cassette (Fig. 2a). To minimize the distance between the mutation and the *piggyBac* transposon, a CTG leucine codon, 10-bp upstream of the mutation, was altered to a TTA leucine codon, generating the TTAA sequence, which would be left in the genome following *piggyBac* excision (Fig. 2b).

Puromycin-resistant human iPSC colonies obtained after co-electroporation of ZFN expression vectors and the targeting vector were screened for targeted clones by PCR. A1ATD-iPSC lines derived from three different patients yielded targeted clones (Table 1). Remarkably, 54% of the puromycin-resistant colonies were targeted on one allele, whereas 4% were the result of simultaneous targeting of both alleles (Supplementary Fig. 1).

To remove the *piggyBac*-flanked selection cassette from these modified clones, we transiently transfected two homozygously targeted clones (B-16 and C-G4) with a hyperactive form of the *piggyBac* transposase[8] and subjected them to FIAU selection. The genotype of the resulting FIAU-resistant colonies was analysed by PCR and confirmed by Southern blot (Fig. 2d and Supplementary Fig. 2a). Biallelic excision was observed in 11% of FIAU-resistant colonies (Table 2). Sequence analyses demonstrated that the *Z* mutation was corrected on both alleles and that transposon excision yielded a TTAA sequence as initially planned (Fig. 2b, e and Supplementary Fig. 2b). The resulting corrected iPSC lines maintained the expression of pluripotency markers for more than 20 passages and their abilities to differentiate into cells expressing markers of the three germ layers (Supplementary Fig. 3), indicating that genome modification did not alter the pluripotency of corrected human iPSCs.

Genomic instability is known to be associated with prolonged culture of human ES cells[20,21] and mutations arising during genome modification would be another concern for clinical application of human iPSCs. Therefore, we analysed the genomic integrity of the human iPSC lines using comparative genomic hybridization (CGH) (Supplementary Table 2a–c). Two out of three A1ATD-iPSC primary lines differed from their parental fibroblasts, showing amplifications or deletions ranging from 20 kb to 1.3 Mb, including a gain of 20q11.21, a frequently

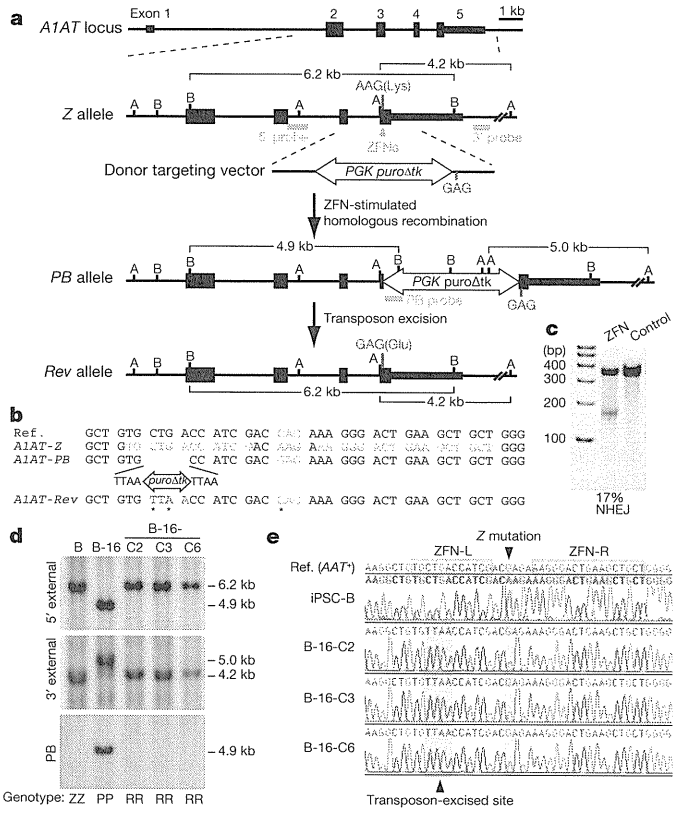

Figure 2 | Correction of the *Z* mutation in human A1ATD-iPSCs. **a**, The strategy for precise genome modification using ZFNs and the *piggyBac* transposon. Top line, structure of the *A1AT* gene; blue lines, Southern blot probes; thin and thick boxes, non-coding and coding exons, respectively; open arrow, *piggyBac* transposon; A, AflIII; B, BamHI. **b**, Sequences of wild-type (Ref.), *Z*, *PB* and *Rev* alleles. Amino acid position 342 (blue), recognition sites for ZFNs (green) and *piggyBac* excision site (red) are shown. Sequence changes in *Rev* allele from *Z* allele are indicated by asterisks. **c**, Surveyor nuclease assay showing the cleavage of the *Z* mutation in ZFN-transfected K562 cells. Non-transfected cells were used as a control. NHEJ, non-homologous end joining. **d**, Southern blot analysis showing biallelic *piggyBac* insertion (B-16) and biallelic excision (B-16-C2, -C3 and -C6) during correction of the A1ATD-iPSC line B. Genomic DNA was digested by BamHI (5′ and PB probes) or AlfIII (3′ probe). Genotype: PP, homozygous for insertion of *piggyBac*; RR, homozygous for reverted allele; ZZ, homozygous for *Z* allele. **e**, Sequence analysis showing correction of the *Z* mutation in three corrected iPSC lines. Wild-type sequence (top line) and A1ATD-iPSC sequence (second line).

amplified region in human ES cells[22,23] (see Supplementary Analysis and Supplementary Fig. 4). Line A retained a normal genome content compared to its parental fibroblast. Reassuringly, we found that after ZFN-stimulated targeting, four out of six homozygous clones had unaltered genomes compared to their parental iPSC lines. Sixteen cell

Table 1 | Summary of PCR genotyping of ZFN-stimulated gene targeting

A1ATD-iPSC line	Clones analysed	Het.*	Homo./Hemi.†	Het. + additional integrations‡	Homo./Hemi. + additional integrations‡	Non-targeted§
A	84	45	3	23	8	5
B	18	10	2	3	3	0
C‖	216	112	9	52	21	22
Mean frequency (%)		54	6	23	12	5

* Het., clones heterozygous for *PB* allele.
† Homo./Hemi., clones homozygous or hemizygous for *PB* allele. Cells with one targeted allele and deletion of the other allele are indistinguishable from correctly targeted homozygous clones by PCR. Such cells are designated as hemizygotes.
‡ Vector backbone integration was analysed by PCR.
§ Clones showing incorrect PCR bands are included.
‖ Sum of two independent experiments.

Table 2 | Frequencies of biallelic *piggyBac* excision

Cell line	Clones analysed	Biallelic excision without re-integration		Biallelic excision with re-integration	
		Number of clones	Frequency (%)	Number of clones	Frequency (%)
B-16	88	15	17	33	38
C-G4	94	5	5	19	20
Mean frequency (%)			11		29

lines with biallelic *piggyBac* excision were compared with their corresponding primary iPSCs and 12 had unaltered genomes. We also analysed the iPSC lines by SNP arrays to check for loss of heterozygosity and found that all lines analysed retained heterozygosity throughout their genome (Supplementary Fig. 5). This observation demonstrates that biallelic gene correction was the result of simultaneous homologous recombination followed by simultaneous excision at both alleles and that mitotic recombination was not involved in this process.

ZFN off-target cleavage and imprecise excision after multiple *piggyBac* transposition might introduce mutations into the genome. To investigate these possibilities at a single base-pair resolution, we sequenced exomes of the corrected B-16-C2 line and its parental fibroblast. Comparison of these exomes identified 29 mutations (Supplementary Table 3). The genesis of these mutations was determined by analysis of the primary iPSC line and the homozygously targeted intermediate. Twenty-four point mutations and one 1-bp deletion were detected in the primary iPSC line and four mutations arose during genetic correction: one during targeting and three during *piggyBac* excision. These mutations seemed to arise during culture as their genomic signatures were inconsistent with ZFN off-target sites or *piggyBac* integration sites (Supplementary Analysis). Taken together, we conclude that the combination of ZFNs with *piggyBac* provides a new method for rapid and clean correction of a point mutation in human iPSCs without affecting their basic characteristics.

To confirm that the genetic correction of A1ATD-iPSCs resulted in the expected phenotypic correction, iPSCs were differentiated *in vitro* into hepatocyte-like cells, the main cell type affected by the disease A1ATD. Differentiation of the corrected lines occurred as expected, resulting in a near homogenous population of hepatocyte-like cells (Supplementary Fig. 6a–c). Remarkably, CGH analysis of differentiated cells showed that hepatic differentiation neither increases the number of genetic abnormalities nor selects for cells with abnormal karyotype (Supplementary Table 2d). The resulting cells shared key functional attributes of their *in vivo* counterparts including glycogen storage, low density lipoprotein (LDL)-cholesterol uptake, albumin secretion and cytochrome P450 activity (Supplementary Fig. 6d–g). Importantly, immunofluorescence and enzyme-linked immunosorbent assay (ELISA) both confirmed the absence of mutant polymeric A1AT in corrected iPSC-derived hepatocyte-like cells that instead efficiently secreted normal endoglycosidase-H-insensitive monomeric A1AT (Fig. 3a–d). In addition, secreted A1AT showed an enzymatic inhibitory activity that was comparable to that obtained from normal adult hepatocytes (Fig. 3e), thereby suggesting that physiological restoration of enzyme inhibitory activity could be achieved.

Lastly, the *in vivo* function of corrected iPSC-derived hepatocyte-like cells (B-C16-2 line) was assessed following transplantation into the liver of *Alb-uPA*$^{+/+}$;*Rag2*$^{-/-}$;*Il2rg*$^{-/-}$ mice via intrasplenic injection. Livers harvested 14 days after injection were colonized by human cells identified using antibodies specific to human albumin and A1AT (Fig. 3f, g). These human hepatocyte-like cells were distributed throughout the liver lobes and were seen to be integrated into the existing mouse parenchyma (Fig. 3f, g). In addition, human albumin was detected in the serum of transplanted animals for at least 5 weeks (Fig. 3h), whereas no tumour formation was detected in any mice. Therefore, corrected iPSC-derived hepatocyte-like cells were able to colonize the liver *in vivo* and show functional activities characteristic of their human ES-cell-derived counterparts[24]. Collectively these analyses

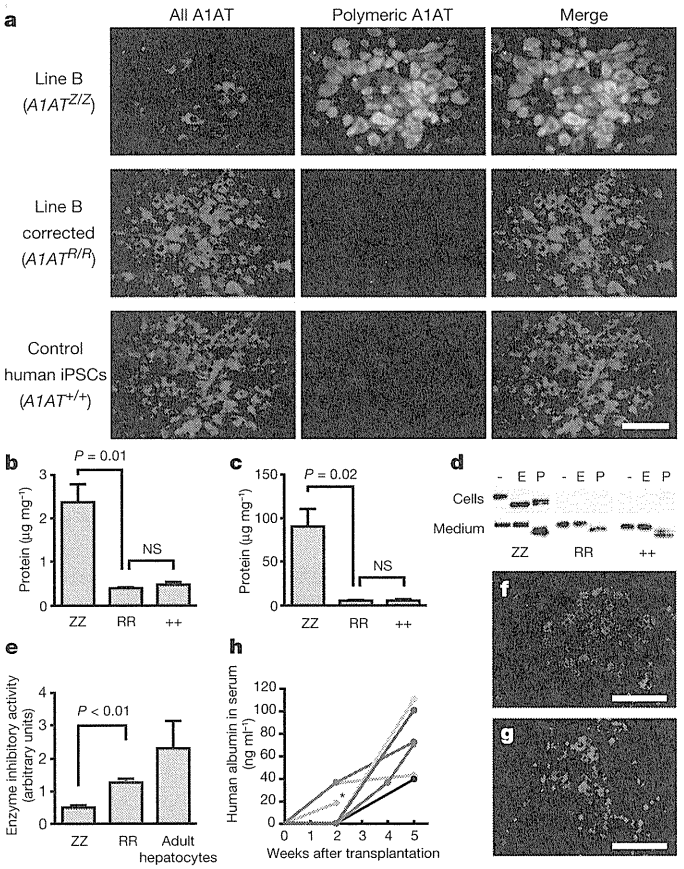

Figure 3 | Functional analysis of restored A1AT in corrected iPSC-derived hepatocyte-like cells. **a**, Immunofluorescence showing the absence of polymeric A1AT protein in hepatocyte-like cells generated from corrected iPSCs. All forms of A1AT (left panels) and misfolded polymeric A1AT (middle panels) are shown. **b**, **c**, ELISA to assess the intracellular (**b**) and secreted (**c**) levels of polymeric A1AT protein in hepatocyte-like cells derived from A1ATD-iPSCs (ZZ), corrected iPSCs (RR) and control human iPSCs (++). NS, not significant. **d**, Endoglycosidase H (E) and peptide:*N*-glycosidase (P) digestion of A1AT immunoprecipitated from uncorrected (ZZ), corrected (RR) and control (++) human iPSC-derived hepatocyte-like cells (upper panels) and corresponding culture medium (lower panels). **e**, Chymotrypsin ELISA showing that corrected cells (RR) have A1AT enzymatic inhibitory activity that is superior to uncorrected cells (ZZ) and close to adult hepatocytes. **f**, **g**, Immunofluorescence of transplanted liver sections detecting human albumin (**f**) and A1AT (**g**). DNA was counterstained with 4′,6-diamidino-2-phenylindole (DAPI). **h**, ELISA read-out of human albumin in the mouse serum longitudinally followed for each mouse. Asterisk, the mouse was subjected to histology analysis. Scale bars, 100 μm. Data in **b**, **c** and **e** are shown as mean ± s.d. ($n = 3$). Student's *t*-test was performed.

demonstrate that genetic correction of the *Z* mutation resulted in functional restoration of A1AT in patient-derived cells.

All the experimental evidence described earlier strongly supports the applicability of genetic correction in patient-specific iPSCs for cell-based therapy of A1ATD. We therefore repeated the genetic correction in more clinically relevant cells using patient-specific iPSCs reprogrammed from fibroblasts with Sendai virus vectors, an integration-free method[25] (Supplementary Fig. 7a–f). One primary human iPSC line with an intact genome by CGH analysis (Supplementary Fig. 7e and Supplementary Table 4) was corrected by the method described earlier. The final product, iPSC-3-G5-A7, had the corrected *A1AT*, an intact genome compared to the parental fibroblast and expressed normal A1AT protein when differentiated to hepatocyte-like cells (Supplementary Fig. 8 and Supplementary Table 4). This is the first demonstration, to our knowledge, of the generation of mutation-corrected patient-specific iPSCs, which could realize the therapeutic promise of human iPSCs.

Here we demonstrate that ZFNs and *piggyBac* transposons enable simultaneous biallelic correction of diseased human iPSCs. No residual ectopic sequences remain at the site of correction and the genome seems to be undisturbed elsewhere. Although we could readily obtain cell lines without large genomic alterations during genetic modification, the resulting corrected human iPSCs carry 29 mutations in protein-coding exons, of which 22 were non-synonymous or splice site mutations. The probable impact of this mutation load needs to be considered in the context of the likely functional impact of the mutations, taking into account the normal germline load, accumulated somatic variation, the presence of compensating normal gene copies and the requirement for the gene product in the derived differentiated cells. From this point of view, only eight mutations might affect gene functions in hepatocyte-like cells (Supplementary Table 3). Nevertheless, the corrected iPSCs could efficiently differentiate to hepatocyte-like cells and engraft into the animal model for liver injury without tumour formation. Therefore, limited genomic abnormalities might have restricted biological consequences. Careful screening of primary and corrected human iPSCs using deep sequencing analyses would contribute to the safe use of human iPSCs in clinical applications.

iPSCs derived from different patients were effectively corrected, demonstrating that this method could be applied to a large number of A1ATD-iPSC lines. Because the biallelic correction could be carried out in less than 4 months, our approach may be compatible with large-scale production of corrected patient-specific iPSCs not only for A1ATD but also for other monogenic disorders.

METHODS SUMMARY

A1ATD-iPSCs were described previously[16]. 2×10^6 human iPSCs were co-transfected with ZFN expression vectors and the donor template, and subjected to puromycin selection (1 $\mu g\,ml^{-1}$) initiated 4 days after transfection. For transposon excision, targeted cells were transfected with pCMV-hyPBase[8], cultured for 4 days, re-plated and selected in 250 nM FIAU. To increase clonogenicity, cells were treated with ROCK inhibitor[26], Y-27632 (10 μM) 4 h before dissociation and 24 h after plating. Resulting colonies were picked 2 weeks later, analysed by PCR and further verified by Southern blot analysis. Primer sequences are listed in Supplementary Table 5.

Full Methods and any associated references are available in the online version of the paper at www.nature.com/nature.

Received 7 January; accepted 8 August 2011.
Published online 12 October 2011.

1. Takahashi, K. *et al.* Induction of pluripotent stem cells from adult human fibroblasts by defined factors. *Cell* **131,** 861–872 (2007).
2. Yu, J. *et al.* Induced pluripotent stem cell lines derived from human somatic cells. *Science* **318,** 1917–1920 (2007).
3. Stadtfeld, M. & Hochedlinger, K. Induced pluripotency: history, mechanisms, and applications. *Genes Dev.* **24,** 2239–2263 (2010).
4. Hanna, J. *et al.* Treatment of sickle cell anemia mouse model with iPS cells generated from autologous skin. *Science* **318,** 1920–1923 (2007).
5. Fairchild, P. J. The challenge of immunogenicity in the quest for induced pluripotency. *Nature Rev. Immunol.* **10,** 868–875 (2010).
6. Tenzen, T., Zembowicz, F. & Cowan, C. A. Genome modification in human embryonic stem cells. *J. Cell. Physiol.* **222,** 278–281 (2010).
7. Urnov, F. D., Rebar, E. J., Holmes, M. C., Zhang, H. S. & Gregory, P. D. Genome editing with engineered zinc finger nucleases. *Nature Rev. Genet.* **11,** 636–646 (2010).
8. Yusa, K., Zhou, L., Li, M. A., Bradley, A. & Craig, N. L. A hyperactive *piggyBac* transposase for mammalian applications. *Proc. Natl Acad. Sci. USA* **108,** 1531–1536 (2011).
9. Wang, W. *et al.* Chromosomal transposition of *PiggyBac* in mouse embryonic stem cells. *Proc. Natl Acad. Sci. USA* **105,** 9290–9295 (2008).
10. Hockemeyer, D. *et al.* Efficient targeting of expressed and silent genes in human ESCs and iPSCs using zinc-finger nucleases. *Nature Biotechnol.* **27,** 851–857 (2009).
11. van der Weyden, L., Adams, D. J. & Bradley, A. Tools for targeted manipulation of the mouse genome. *Physiol. Genomics* **11,** 133–164 (2002).
12. Meier, I. D. *et al.* Short DNA sequences inserted for gene targeting can accidentally interfere with off-target gene expression. *FASEB J.* **24,** 1714–1724 (2010).
13. Lacoste, A., Berenshteyn, F. & Brivanlou, A. H. An efficient and reversible transposable system for gene delivery and lineage-specific differentiation in human embryonic stem cells. *Cell Stem Cell* **5,** 332–342 (2009).
14. Fraser, M. J., Ciszczon, T., Elick, T. & Bauser, C. Precise excision of TTAA-specific lepidopteran transposons *piggyBac* (IFP2) and *tagalong* (TFP3) from the baculovirus genome in cell lines from two species of Lepidoptera. *Insect Mol. Biol.* **5,** 141–151 (1996).
15. Yusa, K., Rad, R., Takeda, J. & Bradley, A. Generation of transgene-free induced pluripotent mouse stem cells by the *piggyBac* transposon. *Nature Methods* **6,** 363–369 (2009).
16. Rashid, S. T. *et al.* Modeling inherited metabolic disorders of the liver using human induced pluripotent stem cells. *J. Clin. Invest.* **120,** 3127–3136 (2010).
17. Perlmutter, D. H. Autophagic disposal of the aggregation-prone protein that causes liver inflammation and carcinogenesis in α-1-antitrypsin deficiency. *Cell Death Differ.* **16,** 39–45 (2009).
18. Gooptu, B. & Lomas, D. A. Conformational pathology of the serpins: themes, variations, and therapeutic strategies. *Annu. Rev. Biochem.* **78,** 147–176 (2009).
19. Zou, J. *et al.* Gene targeting of a disease-related gene in human induced pluripotent stem and embryonic stem cells. *Cell Stem Cell* **5,** 97–110 (2009).
20. Mitalipova, M. M. *et al.* Preserving the genetic integrity of human embryonic stem cells. *Nature Biotechnol.* **23,** 19–20 (2005).
21. Baker, D. E. *et al.* Adaptation to culture of human embryonic stem cells and oncogenesis *in vivo*. *Nature Biotechnol.* **25,** 207–215 (2007).
22. Lefort, N. *et al.* Human embryonic stem cells reveal recurrent genomic instability at 20q11.21. *Nature Biotechnol.* **26,** 1364–1366 (2008).
23. Spits, C. *et al.* Recurrent chromosomal abnormalities in human embryonic stem cells. *Nature Biotechnol.* **26,** 1361–1363 (2008).
24. Touboul, T. *et al.* Generation of functional hepatocytes from human embryonic stem cells under chemically defined conditions that recapitulate liver development. *Hepatology* **51,** 1754–1765 (2010).
25. Fusaki, N., Ban, H., Nishiyama, A., Saeki, K. & Hasegawa, M. Efficient induction of transgene-free human pluripotent stem cells using a vector based on Sendai virus, an RNA virus that does not integrate into the host genome. *Proc. Jpn. Acad., Ser. B, Phys. Biol. Sci.* **85,** 348–362 (2009).
26. Watanabe, K. *et al.* A ROCK inhibitor permits survival of dissociated human embryonic stem cells. *Nature Biotechnol.* **25,** 681–686 (2007).

Supplementary Information is linked to the online version of the paper at www.nature.com/nature.

Acknowledgements We thank A. Klug and M. Minczuk for their advice, M. A. Li for comments on the manuscript, P. Ellis, N. Hammond and C. McGee for CGH analysis, the Sanger Institute sequencing facility for exome sequencing, N. Conte and S. Rice for assistance with bioinformatic analysis, M. Alexander for her help with cell culture reagents. We also thank L. Zhang, S. Hinkley and the production group for ZFN assembly and validation, K. Tong and X. Meng for technical assistance, J. C. Miller and E. Leung for ZFN off-target site analysis and S. Abrahamson and P. D. Gregory for careful reading of the manuscript. This work was supported by the Wellcome Trust (WT077187; A.B.), the MRC Senior non-clinical fellowship and the Cambridge Hospitals National Institute for Health Research Biomedical Research Center (L.V.), the Medical Research Council and Papworth NHS Trust (D.A.L.), the Bill and Melinda Gates Foundation, Inserm and Institut Pasteur (H.S.-M.) and Japan Science and Technology Agency (N.F.). K.Y. is supported by a postdoctoral fellowship of Japan Society for the Promotion of Science. S.T.R. and F.J.R. are Wellcome Trust Clinical Training Fellows. I.V. is supported by a fellowship from the International Human Frontiers Science Program Organization.

Author Contributions K.Y. and S.T.R. are joint first authors. D.A.L., A.B. and L.V. contributed equally to this work. K.Y., S.T.R., D.A.L., A.B. and L.V. conceived the research and wrote the manuscript with comments from all authors. K.Y. performed gene correction in mouse and human iPSCs and conducted all experiments using *piggyBac* in Cambridge, UK. S.T.R., E.M., A.O., N.R.F.H., F.J.R., G.A. and S.J.M. performed *in vitro* phenotypic analysis of corrected human iPSCs. S.T.R., H.S.-M., S.D. and J.P.D.S. performed *in vivo* work. I.V. performed data analysis of exome sequencing. P.Q.-L., D.E.P. and M.C.H. generated and validated ZFNs. N.F. and M.H. generated Sendai virus vectors.

Author Information Exome sequence data have been deposited at the European Genome-Phenome Archive (http://www.ebi.ac.uk/ega/) hosted by the European Bioinformatics Institute under accession EGAS00001000055. CGH and SNP array data have been deposited with EBI ArrayExpress (http://www.ebi.ac.uk/arrayexpress/) under accession number E-MEXP-3316 and with Gene Expression Omnibus (http://www.ncbi.nlm.nih.gov/geo/) under accession number GSE31035, respectively. Reprints and permissions information is available at www.nature.com/reprints. The authors declare competing financial interests: details accompany the full-text HTML version of the paper at www.nature.com/nature. Readers are welcome to comment on the online version of this article at www.nature.com/nature. Correspondence and requests for materials should be addressed to A.B. (abradley@sanger.ac.uk) or L.V. (lv225@cam.ac.uk).

METHODS

Plasmid construction. Gateway-adapted *piggyBac* transposon vectors: a destination vector pPB-R1R2-NP was constructed as follows. The *att*R1 and *att*R2 sites were PCR-generated and digested by NheI/HindIII and XhoI/SpeI, respectively. *EM7-neo* was PCR-generated and digested by HindIII/XhoI. These three fragments were then cloned into the NheI-SpeI site of pPB-LR5 (ref. 27), resulting in pPB-R1R2-Neo. An EcoRI-XbaI fragment containing *PheS* was excised from pR6K-R1R2-ZP[28], blunt-ended and cloned into the blunted XhoI site of pPB-R1R2-Neo, resulting in pPB-R1R2-NP. An entry vector pENTR-*PGKpuroΔtk* was constructed by cloning a KpnI-NotI *PGK-puroΔtk* fragment into the KpnI-NotI site of pENTR-2B.

A targeting vector for *Tyr*: the targeting vector was constructed using BAC recombineering. A bacterial artificial chromosome (BAC) clone RP24-221M7 was introduced into *Escherichia coli* strain EL350 (ref. 29). A mini targeting vector was first constructed to modify the *Tyr* gene on the BAC. Left and right homology arms were PCR-generated and digested by AscI/BsiWI and NsiI/PacI, respectively. The transposon fragment was excised from pPB-R1R2-NP by NsiI/BsiWI digestion. These three fragments were then cloned into the AscI/PacI site of pMCS, resulting in pMCS-Tyr-NP. An AscI-PacI fragment was excised from pMSC-Tyr-NP and used for BAC targeting. A retrieving vector was constructed by cloning PCR-generated left and right homology arms into the XhoI/AscI site of pMSC-DTA, following AscI/HindIII and XhoI/HindIII digestion of the left and right arm, respectively. The retrieving vector was linearized by HindIII digestion and used to retrieve the 3.0-kb 5′ arm, the transposon and the 6.5-kb 3′ arm. Lastly, the *Neo-PheS* cassette was replaced with the *PGK-puroΔtk* cassette by Gateway cloning, resulting in pDTA-Tyr^{PB}. The targeting vector was linearized by AscI before electroporation into the albino miPSCs.

A donor template vector for *A1AT*: a 2-kb fragment, which contained 1 kb on both sides of the Z mutation, was first PCR-amplified using genomic DNA from A1ATD-iPSC line B as a template and cloned into pCR4-blunt-TOPO (Invitrogen), resulting in pCR4-AAT_Z. To construct a donor template with corrected sequence and a *piggyBac* transposon, the 5′ arm and 3′ arm were PCR-amplified and digested with AscI/NsiI and BsiWI/PacI, respectively. The NsiI-BsiWI fragment containing a *piggyBac* transposon with the *Neo-PheS* cassette was excised from pPB-R1R2-NP. The digested fragments were cloned into the AscI-PacI site of pMCS, resulting in pMCS-AAT-PB:NP. The *Neo-PheS* cassette was subsequently replaced with a *PGK-puroΔtk* cassette by Gateway cloning, resulting in the final donor vector, pMCS-AAT-PB:*PGKpuroΔtk*.

The plasmids (pPB-R1R2-NP, pENTR-*PGKpuroΔtk*, pMCS-AAT-PB:*PGKpuroΔtk*) have been deposited in the Wellcome Trust Sanger Institute Archives and are available upon request (http://www.sanger.ac.uk/technology/clonerequests/).

Cell culture. Appropriate ethical approval and patient consent were obtained (Ethics reference no. 08/H0311/201; R&D no. A091485). A1ATD-iPSCs (ref. 16; A, patient 2 line 1; B, patient 1 line1; C, patient 3 line 1) were cultured on mouse embryonic fibroblast (MEF)-feeder layers in human ES cell medium: DMEM/F12 supplemented with 20% knockout serum replacement, 1 mM GlutaMax, 0.1 mM 2-mercaptoethanol, 1× non-essential amino acids and 4 ng ml^{-1} FGF2 (Invitrogen). Subculture was performed every 5–7 days by detaching human iPSCs by incubation in 0.5 mg ml^{-1} dispase and 0.5 mg ml^{-1} collagenase type IV for 1 h at 37 °C, collecting detached human iPSC colonies, breaking down into small clamps and plating them onto new feeder plates. MEFs (CF1 or B6129F1) were cultured in DMEM containing 10% FCS, 2 mM glutamine, 0.1 mM 2-melcaptoethanol and 1× non-essential amino acids. Mouse iPSCs (iPS25Δ1; ref. 15) were cultured on MEF-feeder layers in mouse ES cell medium: KO-DMEM supplemented with 15% FBS, 1 mM GlutaMax, 0.1 mM 2-mercaptoethanol, 1× non-essential amino acids and 1,000 unit ml^{-1} LIF (Millipore).

Gene targeting and transposon excision in mouse iPSCs. 1×10^7 cells were electroporated with 25 μg of a linearized targeting vector in 800 μl of HEPES-buffered saline using a Gene Pulser II electroporator (230 V, 500 μF) and plated onto three 10-cm dishes. The next day, puromycin selection (1 μg ml^{-1}) was initiated. Resulting colonies were picked and screened by PCR. Targeted clones were expanded and further verified by Southern blot analysis. Correctly targeted clones were then subjected to transposon excision. 2×10^6 cells were electroporated with 40 μg of pCMV-hyPBase in 800 μl of HEPES-buffered saline using a Gene Pulser II electroporator (230 V, 500 μF) and plated onto one well of a 6-well plate. After passage once, cells were replated on day 4 at 5×10^5 cells per 10-cm dish. On the following day, FIAU (0.2 μM) selection was initiated. On day 5 of selection, FIAU was withdrawn. Resulting colonies were picked at day 7 and screened by PCR. Primer sequences to detect homologous recombination are shown in Supplementary Table 5.

ZFN-mediated gene targeting in A1ATD-iPSCs. On the day of electropolation (day 0), near-confluent cells were pre-treated with a ROCK inhibitor[26] (Y-27632, Sigma) at 10 μM for 3–4 h before electroporation. Cells were then washed with PBS once, detached by Accutase (Millipore; 10 min at 37 °C) and mixed with DMEM/F12 containing 10% FCS. Cells were dissociated into single-cell suspension by vigorous pipetting and counted. 2×10^6 cells were pelleted and mixed with 5 μg of a 5′-ZFN expression vector, 5 μg of a 3′-ZFN expression vector and 2 μg of the donor template in 100 μl of human ES cell solution 1 (Lonza). The cell suspension was transferred to a cuvette and electroporated using the Amaxa Nucleofector device (Lonza) with program A23. The electroporated cells were plated onto one or two 10-cm feeder dishes in MEF-conditioned human ES cell medium containing 10 μM Y-27632. Human ES cell medium without any drug was used for daily medium change between days 1–3. On day 4, puromycin selection (1 μg ml^{-1}) was started. On day 6, medium was changed to MEF-conditioned human ES cell medium containing 0.5 μg ml^{-1} puromycin, which was used for medium change at every other day until picking colonies. Resulting colonies were picked on day 13–17. Colonies were cut into two pieces. One half was transferred onto one well of a 24-well feeder plate and the other half was lysed and used for PCR genotyping. PCR-positive clones were further expanded and homologous recombination was verified by Southern blot analysis.

Transposon excision in homozygously targeted human iPSCs. Homozygously targeted clones (B-16, C-G4, SeV-1-C3 and SeV-3-G5) were used for transposon removal. Line-A-derived clones were omitted because this line showed a lower capability of differentiating into endodermal lineages. Cells were prepared as described earlier. 2×10^6 cells were mixed with 10 μg of the hyperactive *piggyBac* transposase expression vector (pCMV-hyPBase[8]) in 100 μl of human ES cell solution 1 and electroporated using the Nucleofector device with the program A23. Electroporated cells were plated onto a 6-well plate in 1:2, 1:3 and 1:6 dilutions in MEF-conditioned human ES cell medium containing 10 μM Y-27632. Note that ROCK inhibitor was added to the culture medium until day 6 in this experiment. On day 2, cells with ~80% confluency were passaged using Accutase at a split ratio of 1:2, 1:3 and 1:6 into 6-well plates. On day 4, cells with ~80% confluency were washed with PBS, detached with Accutase, suspended in human ES cell medium and pelleted. Cells were resuspended in human ES cell medium into single-cell level and counted. 1×10^4 cells were then plated onto one 10-cm dish in human ES cell medium containing 10 μM Y-27632. 16–18 h after plating (day 5), medium was changed to human ES cell medium containing 0.25 μM FIAU and 10 μM Y-27632. On day 6, medium was changed to human ES cell medium containing 0.25 μM FIAU and then medium was changed every other day. Genotype and deletion of the *piggyBac* transposon were analysed by PCR and further verified by Southern blot analysis.

CGH analysis. Genomic DNA was extracted using a DNeasy kit (Qiagen). Agilent 244K human genome arrays were used following the manufacturer's protocol. The arrays were scanned with an Agilent microarray scanner and data were generated by Agilent Feature Extraction software. CGH calls were made with Agilent's DNA analytics software using the ADM2 algorithm (6.0 threshold) with a minimum of 5 probes in the region as a filter.

SNP analysis. An Illumina HumanCytoSNP-12 SNP array was used following the manufacturer's protocol. Genotype calls were performed by Illumina's GenomeStudio. B allele frequency and log R ratio were analysed by KaryoStudio. CNVpatition v2.4.4 bundled in KaryoStudio was used for copy number analysis.

ZFN design. ZFNs were designed against a region containing the *Z* mutation in the *A1AT* gene (see Fig. 2a, b) and assembled as previously described[30]. The amino acid residues at positions '−1' to '+6' of the recognition α-helix[31,32] of each of the zinc finger DNA-binding domains for each DNA triplet target are shown in Supplementary Table 2. The ZFNs were linked to the wild-type *Fok*I catalytic domain. The activity of the ZFN at the endogenous target site was determined using the Surveyor Nuclease assay as previously described[33].

Human iPSC-derived hepatocyte-like cell transplantation. All mice were housed in pathogen-free conditions and animal studies were approved by the committee on animal experimentation of the Institut Pasteur and by the French Ministry of Agriculture. Differentiated cells (5×10^5 cells per animal in 50 μl DMEM) were injected into the spleens of 3- to 4-week-old *Alb-uPA*$^{+/+}$;*Rag2*$^{-/-}$;*Il2rg*$^{-/-}$ mice ($n = 7$). The recipient mouse was killed 2 weeks after transplantation for histological analysis. Blood samples were collected and human albumin in plasma was quantified by ELISA (Bethy Laboratories). Frozen liver sections were analysed by immunofluorecence with human albumin (Dako) or human A1AT (Dako) specific antibodies. Non-transplanted mice were used as controls.

Exome sequencing. The corrected iPSC line, B-16-C2, and its parental fibroblasts were analysed. Exome sequencing and analysis were performed as described previously[34] with minor modifications. Exome pull-down was performed using an Agilent SureSelect Human All Exon 50Mb Kit according to the manufacturer's instructions. Enriched DNA was sequenced on an Illumina HiSeq 2000 (75-bp paired-end sequencing). 90.32% (Fibroblast-B) and 90.72% (B-16-C2) of total targeted regions were covered with more than 10× sequencing depth,

covering 93.01% and 93.35% of CCDS exons, respectively. Substitutions in the coding sequence were called as positions with at least 20% of reads reporting a different base with respect the reference human sequence (GRCh37). Additionally, somatic mutations were identified by comparing the sequence with the control fibroblasts, and removing the common polymorphisms described in dbSNP and in the 1000 Genomes Project[35]. Small insertions and deletions were identified using samtools, as the ones not present in the control cell line and that had at least 20× of coverage and 20% of the reads reporting the mutation. Validation of mutations was carried out by Sanger capillary sequencing on parental Fibroblast-B, A1ATD-iPSC line B, the homozygously targeted B-16 cells and the *piggyBac*-excised B-16-C2 cells.

Other experimental procedures. Sendai virus regrogramming, RT–PCR, quantitative RT–PCR, bisulphite sequencing, immunostaining, flow cytometric analysis, ELISA and EndoH analysis were performed as described previously[16,24,25,36].

27. Cadinanos, J. & Bradley, A. Generation of an inducible and optimized *piggyBac* transposon system. *Nucleic Acids Res.* **35,** e87 (2007).
28. Skarnes, W. C. *et al.* A conditional knockout resource for the genome-wide study of mouse gene function. *Nature* **474,** 337–342 (2011).
29. Liu, P., Jenkins, N. A. & Copeland, N. G. A highly efficient recombineering-based method for generating conditional knockout mutations. *Genome Res.* **13,** 476–484 (2003).
30. Urnov, F. D. *et al.* Highly efficient endogenous human gene correction using designed zinc-finger nucleases. *Nature* **435,** 646–651 (2005).
31. Beerli, R. R. & Barbas, C. F. III Engineering polydactyl zinc-finger transcription factors. *Nature Biotechnol.* **20,** 135–141 (2002).
32. Pavletich, N. P. & Pabo, C. O. Zinc finger-DNA recognition: crystal structure of a Zif268-DNA complex at 2.1 Å. *Science* **252,** 809–817 (1991).
33. Guschin, D. Y. *et al.* A rapid and general assay for monitoring endogenous gene modification. *Methods Mol. Biol.* **649,** 247–256 (2010).
34. Varela, I. *et al.* Exome sequencing identifies frequent mutation of the SWI/SNF complex gene *PBRM1* in renal carcinoma. *Nature* **469,** 539–542 (2011).
35. The 1000 Genomes Project Consortium. A map of human genome variation from population-scale sequencing. *Nature* **467,** 1061–1073 (2010).
36. Seki, T. *et al.* Generation of induced pluripotent stem cells from human terminally differentiated circulating T cells. *Cell Stem Cell* **7,** 11–14 (2010).

Efficient generation of transgene-free human induced pluripotent stem cells (iPSCs) by temperature-sensitive Sendai virus vectors

Hiroshi Ban[a,1], Naoki Nishishita[b,c,1], Noemi Fusaki[a,d,2], Toshiaki Tabata[a], Koichi Saeki[a], Masayuki Shikamura[c], Nozomi Takada[c], Makoto Inoue[a], Mamoru Hasegawa[a], Shin Kawamata[b,c,2], and Shin-Ichi Nishikawa[b,c]

[a]DNAVEC Corporation, Tsukuba, Ibaraki 300-2611, Japan; [b]RIKEN Center for Developmental Biology, Kobe, Hyogo 650-0047, Japan; [c]Foundation for Biomedical Research and Innovation, Kobe, Hyogo 650-0043, Japan; and [d]Precursory Research for Embryonic Science and Technology, Japan Science and Technology Agency, Kawaguchi, Saitama 332-0012, Japan

Edited by Yuet Wai Kan, University of California San Francisco School of Medicine, San Francisco, CA, and approved July 7, 2011 (received for review March 21, 2011)

After the first report of induced pluripotent stem cells (iPSCs), considerable efforts have been made to develop more efficient methods for generating iPSCs without foreign gene insertions. Here we show that Sendai virus vector, an RNA virus vector that carries no risk of integrating into the host genome, is a practical solution for the efficient generation of safer iPSCs. We improved the Sendai virus vectors by introducing temperature-sensitive mutations so that the vectors could be easily removed at non-permissive temperatures. Using these vectors enabled the efficient production of viral/factor-free iPSCs from both human fibroblasts and CD34$^+$ cord blood cells. Temperature-shift treatment was more effective in eliminating remaining viral vector-related genes. The resulting iPSCs expressed human embryonic stem cell markers and exhibited pluripotency. We suggest that generation of transgene-free iPSCs from cord blood cells should be an important step in providing allogeneic iPSC-derived therapy in the future.

regenerative medicine | nonintegrating RNA vector

Safer and more efficient reprogramming methods have been explored since the first report of the generation of human induced pluripotent stem cells (iPSCs) (1, 2). Toward this end, several techniques have been used for obtaining integration and/or transgene-free iPSCs, including the use of plasmids (3, 4), the Cre/loxP system (5, 6), adenoviruses (7), piggyBac (8, 9), minicircle vector (10), and proteins (11, 12). However, these methods suffer from low efficiency, require repetitive induction, and/or produce insufficient excision of integrated vectors. Synthetic modified mRNA may solve the problem, but the reagents must be added every day (13). Thus, more efficient and simple methods are needed to generate human iPSCs with no noise of integration or remaining factors for both clinical applications and basic studies.

An alternative technology involves the use of Sendai virus (SeV) vectors. SeV, a member of the *Paramyxovirdae* family, is an enveloped virus with a single-stranded, negative-sense, nonsegmented RNA genome of ~15 kb (14). Importantly, recombinant SeV vectors replicate only in the cytoplasm of infected cells and do not go through a DNA phase or integrate into the host genome (15). SeV vectors have proven to be efficient for the introduction of foreign genes in a wide spectrum of host cell species and tissues, and SeV vectors have been studied for applying to clinical studies of gene therapy for cystic fibrosis, critical limb ischemia, vaccines for AIDS, and other areas (reviewed in ref. 16). We previously reported that the SeV vectors efficiently generate human iPSCs from human fibroblasts (17) and human blood cells (18). However, to apply SeV vector technology to the generation of safer iPSCs, the issue of the sustained cytoplasmic replication of viral vectors after the iPSCs have been established had to be overcome, even though viral vectors are slowly diluted during the robust cell division of iPSCs and SeV vector–positive cells can be removed using an anti–SeV-HN antibody (17). In other words, a more efficient shutdown of viral replication is needed to generate human iPSCs. We considered the use of temperature-sensitive (TS) SeV vectors the likeliest best solution.

Here we show that by introducing point mutations in the polymerase-related genes, we obtained new TS vectors and efficiently generated viral/factor-free human iPSCs from fibroblasts using these vectors by two strategies, (*i*) replacing the MYC vector only and (*ii*) replacing all reprogramming vectors to the TS vectors. We also applied this method to CD34$^+$ cord blood (CB) cells because SeV vector provides a highly efficient gene transfer into human CB-derived hematopoietic stem cells (19). CD34$^+$ CB cells are the youngest somatic stem cells and are expected to have no postnatal genomic aberration by irritants from the environment or UV rays. They correspond to the hematopoietic stem cells and progenitors with less epigenetic modification related to hematopoietic differentiation. These unique features of CD34$^+$ CB cells suggest that this cell fraction might be an ideal cell source fraction for generating a gold standard iPSC. However, the risk of foreign gene integration (20, 21) needs to be overcome for future clinical applications. We successfully obtained viral/factor-free CB-iPSCs by the TS SeV vectors, and examined the advantages of using the TS SeV vector.

Results

Generation of TS SeV Vectors. The SeV RNA polymerase comprises the phosphoprotein (P) and the large protein (L), and formation of the P-L complex is required for RNA synthesis (14). Mutations in P or L have been shown to confer temperature sensitivity to the virus (22, 23). Although a conventional nontransmissible F protein-deficient (ΔF)/TS vector was demonstrated to have low cytotoxicity at temperatures above 37 °C (24), it still expressed the *GFP* gene at 39 °C, albeit at slightly lower levels (Fig. 1*B*). Thus, we generated a greater number of TS vectors using combination of known point mutations in the *P* and/or *L* genes and screened for *GFP* gene expression in infected cells

Author contributions: N.N., N.F., S.K., and S.-I.N. designed research; H.B., N.N., N.F., M.S., N.T., and S.K. performed research; N.F., T.T., K.S., M.I., M.H., S.K., and S.-I.N. analyzed data; and N.F. and S.K. wrote the paper.

Conflict of interest statement: H.B., T.T., K.S., M.I., and N.F. are employees of DNAVEC Corporation. M.H. is a founder of DNAVEC Corporation.

This article is a PNAS Direct Submission.

Freely available online through the PNAS open access option.

Data deposition: The data reported in this paper have been deposited in the Gene Expression Omnibus (GEO) database, ww.ncbi.nlm.nih.gov/geo (accession nos. GSE24240 and GSE25090).

[1]H.B. and N.N. contributed equally to this work.

[2]To whom correspondence may be addressed. E-mail: nfusaki@dnavec-corp.com or kawamata@cdb.riken.jp.

This article contains supporting information online at www.pnas.org/lookup/suppl/doi:10.1073/pnas.1103509108/-/DCSupplemental.

at various temperatures. The TS vectors obtained were (*i*) P2 vectors (D433A, R434A, and K437A), which contain a charge-to-alanine mutation in the L-binding domain of the P protein (22); (*ii*) TS7 vectors (Y942H, L1361C, and L1558I); (*iii*) TS13 vectors (P2 and L1558I); and (*iv*) TS15 vectors (P2, L1361C, and L1558I), as indicated in Fig. 1. In the present study, we chose to evaluate these candidate vectors with combined mutations, because a single mutation appeared to be insufficient to confer temperature sensitivity (i.e., the Y942H, L1558I, or L1361C vector). Furthermore, by using TS candidates with combined mutations, the occurrence of WT revertant, as occasionally observed in RNA viruses (14), was less likely. In contrast with the conventional SeV vector, the TS7 and TS13 vectors expressed *GFP* at 32 °C and 35 °C, and weakly at 37 °C, but not at nonpermissive temperatures of 38 °C or 39 °C. The TS15 vector exhibited greater temperature sensitivity; with this vector, *GFP* expression was barely detected at 37 °C (Fig. 1*B*). We confirmed that there was no *GFP* expression after transfection of cells with the TS7 and TS13 vectors after temperature-shift treatment to 39 °C, even when the infected cells were then cultured at 37 °C for >1 mo with several passages (Fig. 1*C*). None of the vectors was cytotoxic, and all infected cells were attached and live, with or without temperature-shift treatment. Thus, we used these TS vectors to generate human iPSCs.

Generation of Human iPSCs with TS SeV Vectors from Fibroblasts. To apply the TS vectors to generate human iPSCs, we adopted two strategies, (*i*) to replace only *c-MYC*–carrying vector and (*ii*) to replace all of the four gene-carrying SeV vector mixtures to the TS vectors. Our previous study showed that the exogenous *c-MYC* inserted between the *HN* and *L* positions in the SeV vector (*HNL-MYC*) persisted in the infected cells longer than any other vectors carrying *OCT3/4, SOX2*, or *KLF4* at the top of the vectors (18+). When *c-MYC* was inserted at the 18+ position, such selective retention of the c-*MYC*–carrying vector was not observed. This was apparently due to the prolonged replication of the *HNL-MYC* vector (17). Because GFP expression with the TS vectors was relatively weak compared with that obtained using conventional vectors (Fig. 1*B*), we initially inserted *HNL-MYC* into the TS vectors so that the initial levels of expression could be restored by the polymerases supplied in trans from the other vectors (*OCT3/4*, *KLF4*, and *SOX2*). In addition, it was hoped that by using this strategy, the viral vectors might easily disappear when the remaining vector was *HNL-MYC* in the TS vector alone (Fig. 2*A*). Using these vectors at a multiplicity of infection (MOI) of 3, we obtained colonies from human fibroblast cells that were alkaline phosphatase (ALP)-positive and exhibited human embryonic stem (ES) cell-like morphology ~28 d after induction (Fig. 2*B* and Table S1). We then monitored the amount of the SeV genome present during reprogramming and cell expansion using quantitative RT-PCR (qRT-PCR). Surprisingly, replacement of the *HNL-MYC* vector into only one of the four reprogramming factor mixtures using the TS vectors resulted in a marked decrease in all viral genomes after the appearance of the iPSCs (Fig. 2*C*). As expected, expression of *c-MYC* on the TS vectors was correlated with the viral genome (Fig. S1). Then individual colonies were isolated, and the remaining SeV genome in each colony was evaluated. During cell expansion, the vectors were diluted, and most colonies were only partially positive for SeV (Fig. 2*D*, *Middle*). At passage 4, 80% of the colonies were negative for the viral genome using the TS13-

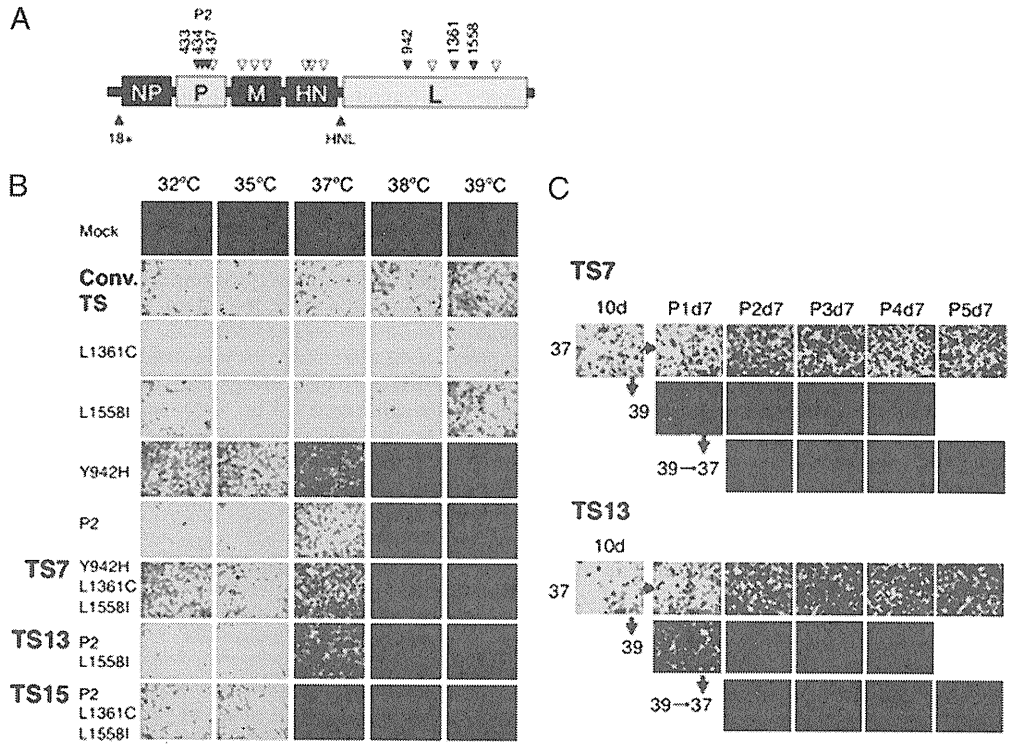

Fig. 1. Generation of TS SeV vectors and inactivation after temperature-shift treatment. (*A*) Point mutations were introduced into the polymerase-related genes *P* (P2: 433, 434, and 437) and/or *L* (942, 1361, and 1558), as indicated in the schematic structure of the ΔF/SeV vector. Open angles indicate conventional mutations in the previous TS vector; closed angles, newly introduced mutations. (*B*) Confluent LLC-MK2 cells were transduced with each SeV vector carrying *GFP* at an MOI of 5 and cultured at the indicated temperatures (32, 35, 37, 38, and 39 °C). Green fluorescence was compared at 3 d after infection. (*C*) To confirm the irreversible inactivation of gene expression by temperature-shift treatment, infected cells were cultured at 37 °C for 10 d and then split into two groups, one group cultured at 37 °C and the other cultured at 39 °C for 28 d, with cells passaged every 7 d. Similarly, cells infected with a TS vector treated at a nonpermissive temperature of 39 °C for 7 d were also cultured for a further 28 d at 37 °C, with cells passaged every 7 d, to evaluate *GFP* expression.

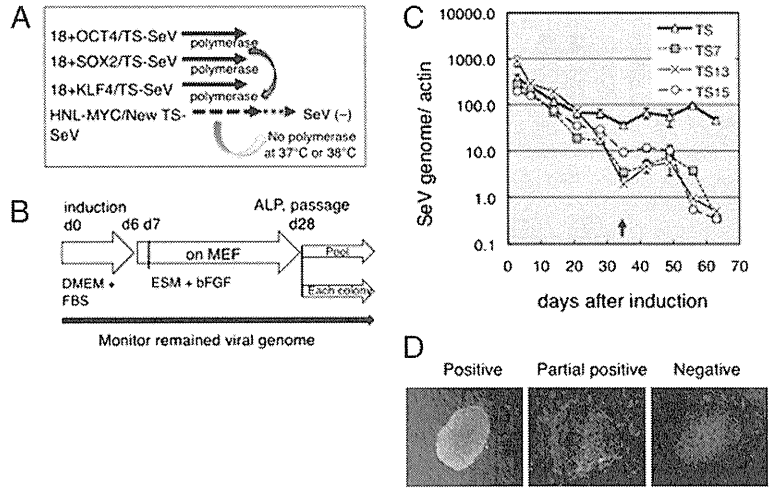

Fig. 2. (*A*) Strategy used to obtain vector/factor-free iPSCs with an SeV vector mixture. Human fibroblasts were infected with the SeV vector mixture containing four factors. During reprogramming, polymerases may be supplied to the TS vector (which has *c-MYC* at the HNL position) by *OCT3/4-*, *SOX2-*, and *KLF4*-carrying conventional SeV vectors. Then the SeV vector may disappear when there is TS vector alone at nonpermissive temperature. (*B*) Procedure for reprogramming using SeV vectors. (*C*) qRT-PCR of existing SeV genomes in induced cells. RNA was extracted from cells between 3 d and 2 mo after infection, and the amount of SeV genome was analyzed by qRT-PCR. iPSC colonies were passaged every 7 d after day 35 (arrow), and whole colonies on the culture dish were analyzed. (*D*) Typical staining of iPSC colonies with anti-SeV antibodies. (*Left*) At passage (P) 1, many colonies were positive for SeV. (*Middle*) After several passages (P4), many colonies were partially positive. (*Right*) Colonies were found to be negative for SeV at P10. (Scale bar: 200 μm.)

HNL-MYC and TS15-*HNL-MYC* vectors, and by passage 10, all colonies were negative for the vector by qRT-PCR (Fig. 3*A*, *Left*). Because the number of SeV-negative colonies was not increased using the TS7 vector at passage 10, although the partial negative colonies were increased, the iPSCs were subjected to a temperature shift to 38 °C (Fig. 3*A*, *Right*). Incubation of cells at 38 °C for 3–5 d was sufficient to obtain SeV-negative iPSCs (Figs. 3*A* and 4*B*) with no changes in the expression of human ES cell (hESC) marker genes, *NANOG* (Fig. 4*B*), or the other related marker genes. Quantitative RT-PCR analysis and Western blot analysis of these iPSCs obtained by the first strategy revealed no detectable viral genome or protein expression in the established iPSCs at the late passage numbers, with slightly detectable viral genome or protein expression in the pooled colonies at passage 8 (1/1,000–1/10,000 compared with day 3; Fig. 3 *B* and *C* and Table S3). TS15 showed higher dilution than other vectors, comparable to their temperature sensitivities. More importantly, copy numbers of *OCT3/4, SOX2, KLF4*, and *c-MYC* genes in SeV-generated iPSCs were the same as in parental cells, in contrast to retroviral-generated iPSCs, in which copy numbers were verified because of the vector integration (Fig. 3*D*). The condition and the efficiencies of these experiments and characteristics of obtained iPS clones are summarized in Tables S1 and S3.

Expression of Human ES Cell Markers and Epigenetics. All iPSCs examined expressed hESC markers, as determined by qRT-PCR, and were positive for stage-specific embryonic antigen (SSEA)-4, TRA-1-60, TRA-1-81, NANOG, and OCT4, as demonstrated by immunostaining (Fig. S2 *A* and *B*). Furthermore, CpG dinucleotides at the *OCT3/4* promoter region in the iPSCs were demethylated (Fig. S2*C*). Global gene expression in the iPSCs was similar to that of hESCs (Fig. S3*A*). Clustering analysis revealed a high degree of similarity among the reprogrammed iPSCs obtained using the TS7, TS13, or TS15 vectors that clustered together with hESCs and was distant from that of the parental somatic cells. These iPSCs had a normal 46 XY or 46 XX karyotype, even after temperature-shift treatment, and could be maintained for more than 20 passages (Fig. S4*A* and Table S3). DNA fingerprinting analysis verified that these iPSCs were indeed derived from the parental fibroblast cells (Fig. S4*B*).

Established iPSCs Show Potentiality of Differentiation to Three Germ Layers. The ability of hESCs/iPSCs to differentiate into all cell types provides the basis for their potential in regenerative medicine. Thus, we investigated the differentiating potential of SeV-generated iPSCs by evaluating teratoma formation. In these experiments, the virus-negative iPSCs were injected s.c. or i.m. into NOD/SCID mice. Histological examination of the teratomas revealed that the tissues had originated from the three embryonic germ layers and included neural and epithelial tissues, muscle, cartilage, bone, gut-like structures, and various glandular structures (Fig. S3*B*). We further tested the pluripotency of SeV-generated iPSCs in vitro. Like hESCs, these iPSCs formed embryoid bodies in suspension culture (Fig. S4*C*). For mesoderm-derived differentiation, the embryoid bodies were grown in adherent culture with 0.1 mM ascorbic acid and 20% FBS to enhance cardiomyocyte differentiation (25), whereas an established protocol for hESCs involving activin A treatment (26) was used for the induction of definitive endoderm cells. As a result, SeV-generated iPSCs differentiated into beating cardiomyocytes and endoderm-derived pancreatic cells that stained positive for pancreatic and duodenal homeobox 1 (PDX1; Fig. S4*C*). Coculture of these iPSCs with PA6 feeder cells resulted in the generation of dopaminergic neurons (ectoderm derivatives) that were positive for βIII tubulin and tyrosine hydroxylase (27) (Fig. S4*C*). These data indicate that the SeV-generated iPSCs are pluripotent, like hESCs, and respond to different differentiation stimuli. Based on these results, we conclude that the viral/factor-free iPSCs generated using TS SeV vectors meet the criteria of hESCs and could serve as a clinically important source of stem cells without the danger of integration of any foreign genes.

Generation of Human iPSCs from CB Cells. In the second strategy, we obtained viral-free iPSCs from human fibroblasts using TS13 or TS7 vector mixtures consisting of four reprogramming factors (i.e., 4F/TS13 and 4F/TS7, respectively) at a higher MOI of 30 at 37 °C, with (TS7) or without (TS13) temperature-shift treatment (Fig. 4 *A* and *B* and Table S1). In this case, we used a higher MOI because we could not obtain iPSCs at a lower MOI, likely due to the weak expression of TS vectors at 37 °C, lacking any supplemental polymerases from mixed conventional vectors. However,